S100P DISSOCIATES MYOSIN IIA FILAMENTS AND FOCAL ADHESION SITES TO REDUCE CELL ADHESION AND ENHANCE CELL MIGRATION

Min Du[1], Guozheng Wang[2,4], Thamir M. Ismail[1], Stephane Gross[3], David G. Fernig[1], Roger Barraclough[1] and Philip S. Rudland[1,4]

From Institute of Integrative Biology[1] and Institute of Infection and Global Health [2], University of Liverpool, Crown Street, Liverpool, L69 7ZB, U.K. and School of Life and Health Sciences[3],Aston University, Aston Triangle, Birmingham B4 7ET

Running head: Mechanism of S100P-induced cell migration

Corresponding authors[4]: Guozheng Wang, wangg@liv.ac.uk and Philip Rudland, rudland@liv.ac.uk, Life Science Building, Crown Street, Liverpool, L69 7ZB, UK. Tel: +44 151 7954474.

Key words: S100 proteins; Cell migration; Metastasis; Myosin; Cell adhesion.

Background: Certain S100 proteins induce cell migration and metastasis but the molecular mechanism is not clear
Results: S100P preferentially binds and disperses NMIIA fibres and subsequently affects focal adhesion sites (FAS) and cell adhesion
Conclusion: S100P over-expression reduces the assembly of NMIIA-FAS to enhance cell migration by reducing anchorage forces
Significance: The mechanism of the primary step of S100P-induced metastasis has been elucidated.

SUMMARY

S100 proteins promote cancer cell migration and metastasis. To investigate their roles in the process of migration we have constructed inducible systems for S100P in rat mammary and human HeLa cells that show a linear relationship between its intracellular levels and cell migration. S100P, like S100A4, differentially interacts with the isoforms of nonmuscle myosin II (NMIIA, Kd = 0.5 μM ; IIB, Kd = 8 μM; IIC, Kd = 1.0 μM). Accordingly, S100P dissociates NMIIA and IIC filaments but not IIB in vitro. NMIIA knockdown increases migration in non-induced cells and there is no further increase upon induction of S100P, whereas NMIIB knockdown reduces cell migration whether or not S100P is induced. NMIIC knockdown does not affect S100P-enhanced cell migration. Further study shows that NMIIA physically interacts with S100P in living cells. In the cytoplasm, S100P occurs in discrete nodules along NMIIA-containing filaments. Induction of S100P causes more peripheral distribution of NMIIA filaments. This change is paralleled by a significant drop in vinculin-containing, actin-terminating focal adhesion sites (FAS) per cell. The induction of S100P, consequently, causes significant reduction in cellular adhesion. Addition of a focal adhesion kinase (FAK) inhibitor reduces disassembly of FAS and thereby suppresses S100P-enhanced cell migration. In conclusion, this work has demonstrated a mechanism whereby the S100P-induced dissociation of NMIIA filaments leads to a weakening of FAS, reduced cell adhesion and enhanced cell migration, the first major step in the metastatic cascade.

S100 proteins, such as S100B, S100A2, S100A4, S100A6, and S100P are upregulated in the primary tumors of many cancers, including those of the breast, brain, lung, pancreas, prostate, and colon (1-3). Moreover their overexpression in the primary tumor is often associated with poor patient prognosis and is believed to be due to their ability to induce cell migration and metastasis (4-10). Artificial transfection and thereby upregulation of certain S100 proteins can modulate the cytoskeleton and increase cell migration in many diverse systems

in vitro (11-13). The major molecules of the acto-myosin cytoskeleton in cancer cells are the isoforms of non-muscle myosin IIs (NMIIs), NMIIA, IIB and IIC. NMIIA is associated with organisation of stress fibres, focal adhesion sites (FAS) and tissue architecture (14). NMIIB is involved in stabilising normal cell polarity (15) and is essential for heart and brain development (16,17). NMIIC is a recently discovered isoform whose function is poorly understood (18), but it may share properties with NMIIA and IIB (19).

One S100 protein, S100A4, has been shown to interact with NMIIA (12,20). This interaction directly inhibits the formation of filaments of NMIIA *in vitro* (11) and increases cell migration *in vivo* (21). In contrast, the interaction of S100A4 with NMIIB is much weaker (22). In different cellular systems, when expression of NMIIA is knocked down, cell migration is increased, but when NMIIB is knocked down, cell migration is reduced (23). These observations suggest that S100A4 and perhaps other S100 proteins may interact differentially and regulate these different NMII isoforms to achieve an overall increase in cell migration, but how the overall increase is achieved is unknown. To test how this is brought about, S100P has been used as a representative of the S100 proteins, because its metastasis-promoting property has been well characterised *in vivo* (7) and S100P-inducible cell lines have been successfully established from a rat breast tumor cell line and from HeLa ovarian cancer cells. We now show that S100P also binds preferentially to NMIIA, partially dissociates its filaments and causes their redistribution, and that these changes are companied by a redistribution of FAS, from the central area to the cellular periphery. The number of FAS per cell is also significantly decreased. Consequently cell adhesion is reduced and cell migration is enhanced. These changes suggest that the weakening of the anchorage forces generated through NMIIA to FAS will allow intact NMIIB filaments to drive cell migration.

EXPERIMENTAL PROCEDURES

Cell culture- The Rama 37 cells, a non-metastatic benign rat mammary tumor cell line expressing undetectable levels of S100P, S100P cDNA transfected cell lines (Rama 37-S100P-1, 2; Rama 37 pool-1, 2) and control vector alone transfected cell line (Rama 37-vector), were established and cultured as described previously (7). Human cancer cell lines, HeLa, MCF-7 and MDA-MB-231, cells were cultured routinely (24).

Establishment of doxycycline inducible cell system- The tetracycline inducible system (gifted by Dr. Adam West, NIH, USA) contains two plasmids, pBTE to express a regulatory element rtTA2(S)-M2 (25), and pTRE-ins to express target protein. Two inducible clones derived from Rama 37 cells were termed Rama 37-T25 and T28, while two inducible clones derived from HeLa cells were termed HeLa-A3 and A19. The concentration of doxycycline and induction period was optimised and 1 μg/ml of doxycycline for 24 h was used in all the inductions (Supplemental Fig.1).

Measurement of cell migration- Migration of cell lines was measured 24 h after the cells were seeded in Boyden Chambers using 6.5 mm diameter polycarbonate membrane inserts containing 8 μm pores (Corning Costar, Acton, USA)(26), as described previously (27) . The inducing agent, doxycycline, inhibitors, or blocking peptide and antibodies were added to both upper and lower compartments of the Boyden Chambers. To standardise results between different experiments, usually the cell line controls were set to 100% migration and changes relative to this value were shown in most Figs.

SiRNA transfections- Two siRNA sequences used for targeted silencing of human S100P and four siRNA sequences for each human NMII isoforms, vinculin, Rac1 and RhoA were designed and synthesized by Qiagen (Crawley, UK) (Supplemental Table1). S100P-expressing MCF-7 and HeLa/HeLa-A3/HeLa-A19 cell lines were used for testing S100P siRNAs,NMII siRNAs, vinculin, Rac1 and RhoA siRNAs, respectively. RNAi Starter kit (301799), including RNAiFect, negative control siRNA, were from Qiagen. The siRNA transfection procedure followed Qiagen's instructions. At 48 h after transfection, the levels of S100P, NMIIA IIB (Supplemental Figs. 2A&B), vinculin, Rac1 and RhoA were measured using Western blotting and the levels of NMIIC mRNA (Supplemental Fig. 2C) by semi-quantitative RT-PCR, because there was no satisfactory antibody for NMIIC.

Semi-quantitative RT-PCR- Total RNA was extracted using Trizol reagent (Invitrogen, Paisley, UK). Reverse transcription was carried out using a Cloned AMV First-Strand synthesis Kit (Invitrogen). The resultant cDNA was used as template for the amplification of actin (18

cycle) and NMIIC (25 cycle) by PCR using primers listed in Supplemental Table 2.

Recombinant Proteins- The recombinant human S100P protein was purified as described previously (28,29). The r*C*-NMIIA (*C*-terminal 149aa), IIB (*C*-terminal 204 aa) and IIC (*C*-terminal 178aa) were produced using the same method as used previously for r*C*-NMIIA (30) with primers listed in Supplemental Table 2. The deletion mutants of r*C*-NMIIA, M1, M2, M3, M4, M5, were produced by the PCR extension method (31,32) .

Western blotting- S100P was detected using mouse anti-S100P mAb (1:50 dilution) (BD Science, San Jose, USA), which showed no cross-reaction with S100A1, S100A2 or S100A4 (7). FAK was isolated using anti-FAK conjugated agarose (Millipore, Billerrica, USA) from 1 mg protein prior to SDS-PAGE. NMIIA, IIB, FAK, phospho-FAK (pFAK) and actin were detected using rabbit polyclonal anti-NMIIA, IIB (Covance, Princeton, USA), mAb-FAK and polyclonal anti-pFAK Y(397) (Upstate, New York, USA).

Gel overlay assay- Briefly, equal amounts of proteins (3 µg) were subjected to SDS-PAGE (33). One gel was stained with Coomassie brilliant blue to check equal loading and the other two gels were electro-blotted onto PVDF membranes, which were then incubated at 4^{o}C overnight with S100A4 (3 µg/ml) or S100P (3 µg/ml) in Overlay Buffer (12). The rest of the procedures were the same as those of conventional Western blotting.

Binding assays- Binding reactions were carried out in an IAsys two-channel resonant mirror biosensor (Affinity Sensors, Saxon Hill, Cambridge, U. K.), as described previously (34); the r*C*-NMIIA, IIB or IIC protein fragment was immobilized on aminosilane surfaces using BS^3 (Perbio, Chester, UK). The equilibrium dissociation constant (K_d) was calculated both from the association and dissociation rate constants, and from the extent of binding at or near equilibrium (34).

Sedimentation assay- Briefly, 5 µM of r*C*-NMIIA, IIB or IIC was incubated at 4^{o}C overnight in Bundling Buffer (10 mM imidazole-HCl (pH 7.5), 100 mM NaCl, and 2.5 mM $MgCl_2$)(35). To test the effect of S100P on rC-NMII sedimentation, 0- 10 µM of S100P was pre-incubated with r*C*-NMIIA, IIB or IIC with 0.5 mM $CaCl_2$ at room temperature for 40 min. Bundling Buffer was then added and NaCl and $MgCl_2$ adjusted to 100 mM and 2.5 mM, respectively. Twenty µl of mixture was removed and kept at -20^{o}C as a control, and the remainder was incubated overnight at 4^{o}C. After centrifugation at 13,600 g for 30 min at 4^{o}C, 20 µl of the supernatant was subjected to SDS-PAGE together with control. Anti-His-tag antibody (Sigma) was used to detect r*C*-NMIIA, IIB and IIC by Western blotting. To test if S100P disassociates the preformed NMII filaments, the r*C*-NMIIA, IIB and IIC were incubated in Bundling Buffer for 48 h. After centrifugation, pellets were resuspended in Bundling Buffer containing 0, 3 µM S100P. After 40 min incubation, the mixtures were centrifuged and resultant supernatants were analysed.

Immunofluorescent staining- Culture of the human breast cancer cell line MCF-7 and dual immunofluorescent staining were carried out as described before (24).The cells were grown on the untreated glass surface of 8-well chamber slides (BD Science). S100P was detected with the MAb (BD Science) at 1:50 dilution and visualised with FITC-conjugated goat anti-mouse antibody (Sigma). NMIIA and IIB were detected with rabbit anti-NMIIA and IIB IgGs (Covance, Princeton, USA) at 1:5000 dilution and visualised with Texas Red-conjugated goat anti-rabbit antibody (Molecular Probes, Eugene, USA). Actin filaments were visualized with Atto 647N-Phalloidin (Sigma). FAS were detected with mAb (Sigma) at 1:2000 dilution and visualized as for S100P. Images were recorded using a Zeiss LSM 510 confocal microscope.

Fluorescent lifetime imaging- For fluorescent resonance energy transfer (FRET) analysis, the expression plasmids, pECFP-S100P and pNMIIA-EYFP were constructed by inserting S100P and NMIIA coding sequences into pECFP-C1 vector (Clontech, Palo Alto, CA) and pEYFP-N1 vector (Clontech) at the *Hind*III and *Bam*HI sites, respectively. The correct coding sequences for the two fusion proteins, ECFP-S100P and NMIIA-EYFP were confirmed by DNA sequencing. The pECFP-S100P and the pNMIIA-EYFP/pEYFP-C1 expression vectors were then co-transfected into HeLa cells. The time-resolved fluorescence decay maps were collected pixel-by-pixel from the HeLa cells co-expressing ECFP-S100P and NMIIA-EYFP fusion proteins or from the HeLa cells co-expressing ECFP-S100P and EYFP by a scanning confocal microscope using time-correlated single photon counting (TCSPC) (36) fluorescence

lifetime imaging module (SPC-730) (Becker &Hickl, Berlin, Germany) and a photomultiplier tube (PMH-100-1, Hamamatsu, Bridgewater, USA). Fluorescence lifetime imaging microscopy (FLIM) images were analyzed using SPCImage 2.0 (Becker & Hickl). The methods for calculation of fluorescence lifetime and the distance between donor and acceptor as well as the statistical analysis are fully described elsewhere (37).

Timelapse confocal microscopy- GFP-NMIIA expression plasmid (full length) was obtained from Addgene, Cambridge, USA. The HeLa-A3 was grown on glass bottom dishes (Matsunami Glass, Tokyo, Japan) and transfected with the plasmid using Lipofectamine (Invitrogen). Doxycycline (1 µg/ml) was added to the cell culture 16 h after transfection. Images of transfected cells were recorded in a Zeiss LSM 510 confocal microscope for a further 24 h.

Triton-insoluble NMIIA detection- Equal number of HeLa and HeLa-A19 cells were cultured in the presence or absence of doxycycline for 24 h and washed with ice cold PBS. The cells were then incubated with ice cold cytoskeletal lysis buffer (40 mM sodium pyrophosphate, 20 mM potassium phosphate, 3 mM EGTA (pH 7.4) and 1% Triton X-100 for 5 min on ice. The buffer was then removed to a fresh tube and 20 µl was taken for soluble actin detection. The material remaining on the dish after two washes with the buffer was considered as the detergent-insoluble cytoskeletal fraction and harvested by adding 2xSDS gel loading buffer. The insoluble NMIIA and soluble actin (as a loading control) were detected by Western blotting.

Peptide synthesis and transfer – The S100P binding domain of NMIIA fused with TAT-HA2 (38) was synthesized by GeneCust Europe, (Luxembourg). TAT-HA2 was used as control peptide. HeLa and HeLa-A19 cells were incubated with 5 µM peptides for 24 h. Cell migration assay was set up in the presence or absence of doxycycline.

Cell adhesion assay – A modified attachment assay (39) was carried out. HeLa and HeLa-A19 cells were induced with 1 µg/ml doxycycline for 24 h. The cells were then detached by EDTA which was neutralised by culture medium, washed with PBS and resuspended to 4 x 10^5/ml in basal medium without serum, 50 µl cells were seeded in each well of 96-well microtiter plate (Costar, Cambridge, USA). After incubation in CO_2 incubator at 37 ^oC for 5, 30, 60 or 90 min, the plate was shaken at 2000 rpm for 10-15 seconds and washed with PBS for 3 times. The remaining cells were fixed with 5% (w/v) glutaradehyde. After washing, the cells were stained with crystal violet for 10 min. After washing with water 5 times, the plate was dried and 100 µl 10% (v/v) acetic acid was added. After 30 min incubation, the absorption was recorded at 570 nm. The cell adhesion assay kit was purchased from Millipore and used according to the supplier's instructions.

RESULTS

Regulation of the levels of intracellular S100P affects cell migration. When the rat mammary 37 (Rama 37) cells were transfected with an expression vector for S100P, the resultant transfectants, R37-S100P-1 and R37-S100P-2, and two pooled clones, pool-1 and, pool-2 (7), expressed 6-14 fold of S100P mRNA and 5-12 fold of S100P protein over the pooled empty vector-transfected Rama 37 cells (R37-vector), causing an increase in cell migration of 30-70% (Figs. 1A&B) (ANOVA test, $P<0.01$). To down regulate the levels of S100P, two specific small interference RNAs (siRNAs) to the mRNA for S100P were synthesised and transfected into MCF-7 cells, a human breast cancer cell line that expressed high levels of S100P. The siRNA duplex 1 and 2 separately reduced the levels of S100P in MCF-7 cells to 10% and 80%, respectively and led to a reduction in cell migration of about 45% and 75%, respectively ($P=0.004$ and $P=0.2$) (Figs. 1C&D). To upregulate the levels of S100P, the doxycycline-inducible cell lines, Rama 37-T25, T28 and HeLa-A3 and A19 were constructed from rat mammary benign and human malignant ovarian cells. After addition of 1 µg/ml doxycycline for 24 h, the level of S100P was significantly increased by 5-10 fold ($P\leq0.001$) and that of cell migration by 2-3 fold, respectively ($P\leq0.008$) (Figs. 1E&F). Levels of S100P and migration of Rama 37 and HeLa showed no significant differences with or without inducing agent ($P\geq0.30$; Figs. 1E&F). There was a significant positive correlation between the levels of S100P and cell migration (Supplemental Fig. 3).

Although there is no secretion signalling peptide in any of the S100 proteins, it is thought that the S100 proteins can be secreted and may function at low concentrations of around 100 nM (1 µg/ml)(40,41) by activating the receptor for advanced glycation end-products (RAGE) on the cell surface (42,43). However, S100P was not

detectable in the conditioned medium of doxycycline-induced or non-induced R37-T25 and HeLa-A3 cells (Fig. 1G). When 100 nM human recombinant S100P (rhS100P) was added to Rama 37-T25 or to HeLa-A3 cells (Fig. 1H), it produced no significant increase in cell migration ($P \geq 0.23$), although it significantly increased cell invasion (Du, Wang and Rudland unpublished data). Increasing the dose of rhS100P up to 1 μM did not achieve significant increase of cell migration (data not shown). Moreover, the RAGE neutralising antibody or blocking peptide (8,43) did not significantly inhibit cell migration enhanced by doxycycline-induced S100P (Fig. 1H)($P \geq 0.09$). These data suggest that the upregulation of intracellular S100P, but not the secreted S100P, is the primary cause of S100P-enhanced cell migration at least in those cell lines tested.

Preferential interaction of S100P with NMIIs interferes with their corresponding filament formation. The recombinant *C*-terminal fragments of NMIIA, IIB and IIC (r*C*-NMIIA, B, C) were separately immobilized onto a biosensor and the extent of binding of different concentrations of S100P was measured in a buffer containing 0.5 mM Ca^{2+}. The binding characterized by fast association kinetics was always homogeneous and there was no evidence for more than one binding site for S100P. The equilibrium dissociation constants (K_d) for r*C*-NMIIA, IIB or IIC calculated from these kinetic parameters were: 430±210; 7,800±4,200; and 1,000±530 nM, respectively, very similar to the K_d's calculated from the extent of binding observed at equilibrium of: 500±200; 8,400±1,200; and 490±100 nM, respectively (Table 1). Therefore, the binding affinity of S100P with r*C*-NMIIA is similar to that with r*C*-NMIIC and is 10-20 fold higher than that with r*C*-NMIIB.

Binding of S100A4 has been mapped to amino acids 1909-1937 of NMIIA (20). Since S100P has a similar structure (44,45), the deletion mutant polypeptides of NMIIA (M1-M5) used for mapping S100A4 binding sites (20) were employed for S100P (Figs. 2A-C). Since mutant M1 failed to bind, but mutants M2 and M3 did so to S100P, the region from amino acid 1909 to 1937 of the r*C*-NMIIA is confirmed to be a major sequence for S100P and S100A4 binding (Figs. 2A- C). The additional binding to M3 over M2 (Figs. 2B, C) suggests partial overlap of this binding site with the filament assembly domain which plays an important role in regulating NMIIA filament formation (Fig. 2A)(22,46).

When S100P was pre-incubated with r*C*-NMIIA or IIC, formation of their filaments was inhibited. Thus when mixtures that contained r*C*-NMIIA and S100P were centrifuged, the amount of soluble r*C*-NMIIA retained in the supernatant was significantly increased by about 2 fold for 0.3 μM to 6 fold for 10 μM S100P (ANOVA test, $P<0.01$) (Figs. 2D&E). In contrast, prior incubation of S100P with r*C*-NMIIB showed no significant change ($P>0.05$).When S100P was pre-incubated with NMIIC, the amount of soluble form increased by 6-fold for 3 μM and 10 fold for 10 μM S100P; hence the formation of NMIIC filaments was also significantly inhibited by S100P ($P<0.01$) (Figs. 2D&E). When 3 μM S100P was added to preformed filaments of specific NMII isoforms, S100P significantly increased the amount of soluble forms of NMIIA and IIC by 6 and 2.7 fold on average, respectively (Student's t test, $P \leq 0.007$), but not those of NMIIB ($P=0.25$)(Figs. 2F&G). This result shows that S100P can partially dissociate preformed NMIIA and IIC filaments, but not those of NMIIB.

Knocking down NMII isoforms affects S100P-induced cell migration. When expression of NMIIA was knocked down by over 90% using specific siRNA in HeLa-A3 cells (Supplemental Fig. 2A), cell migration was significantly increased by 64-123% ($P<0.025$)(Fig. 3A, non-induced), while knocking down NMIIB by 80-90% (Supplemental Fig. 2B) significantly reduced cell migration to 31-60% of its original value ($P \leq 0.02$)(Fig. 3B, non-induced). When expression of NMIIC was knocked down by 70% (Supplemental Fig. 2C), cell migration did not change significantly ($P \geq 0.12$)(Fig. 3C, non-induced). When S100P was induced prior to NMIIA knockdown, the subsequent knockdown of NMIIA failed to increase significantly cell migration any further ($P \geq 0.24$)(Fig. 3A, induced) and vice versa ($P \geq 0.21$)(Fig. 3D). When the expression of S100P was induced and then that of NMIIB was knocked down, cell migration was decreased by 47- 83% (Fig. 3B, induced) ($P=0.02$ and $P=0.08$). When NMIIB was knocked down and S100P was then subsequently induced, there was no significant increase in cell migration ($P \geq 0.12$)(Fig. 3E), suggesting that NMIIB could be the major driver of cell migration. Either when S100P was induced before (Fig. 3C, induced) or after (Fig. 3F) NMIIC was knocked down, cell migration was significantly increased by 55-

121% (Student's t test, P≤0.033), which is similar to cells transfected with control siRNA, suggesting that NMIIC fails to play a major role in regulating S100P-enhanced cell migration. These data strongly indicate that S100P increases cell migration mainly through its effect on NMIIA.

Co-localisation and physical interaction of S100P with NMIIA in living cells. In MCF-7 cells, S100P protein was distributed both in the nucleus and in the cytoplasm. Cytosolic S100P was more concentrated in the perinuclear region (Fig. 4A panels A&D), the same as that in green fluorescent protein (GFP)-S100P transfected cells (Supplemental Fig. 4). The cytosolic S100P formed scattered focal densities (Fig. 4A panels A&D). The NMIIA protein occurred in cytosolic filaments (Fig. 4A panels B&E), and also formed nodules along the filaments. Some of these nodules co-localised with the majority of S100P-containing focal densities (Fig. 4A panels C&F). To investigate if S100P physically interacts with NMIIA in mammalian cells, the plasmid expressing enhanced cyan fluorescent protein (ECFP)-S100P fusion protein and the plasmid expressing NMIIA-EYFP (enhanced yellow fluorescent protein) or EYFP alone were co-transfected into HeLa cells. The fluorescent lifetime of ECFP-S100P was measured both from cells co-expressing ECFP-S100P and NMIIA-EYFP (1.12±0.14 ns, mean±SD from 7 different cells in two independent transfections) (Fig. 4B panel A), and cells co-expressing ECFP-S100P and EYFP (2.38±0.07 ns, mean±SD from 5 different cells in two independent transfections) (Fig. 4B panel B). A significant reduction (Student's t test, P< 0.01) in the mean fluorescent lifetime of ECFP-S100P was observed in the cells co-expressing NMIIA-EYFP compared to that of cells co-expressing EYFP (Fig. 4B panel C). The reduction in mean fluorescence lifetime resulted from the transfer of the energy from the optically excited ECFP-S100P to NMIIA-EYFP but not to the EYFP. This indicates that the S100P and NMIIA were in physical contact, i.e. < 5 nm apart (47,48). These data confirmed that the *in vitro* interactions between S100P and NMII isoforms also occur *in vivo*.

S100P induces reorganisation and reduces the total amount of NMIIA filaments in living cells. GFP-tagged full length NMIIA (Fig. 5A) was expressed in HeLa-A3 and A19 cells by transient transfection. Doxycycline was added at 16 h after transfection. At that time, NMIIA filaments were visible and distributed uniformly in the majority of GFP-fluorescing cells, with only 7-10% showing a peripheral distribution (Supplemental Table 3). About 5% of fluorescing cells had no obvious filaments or only aggregated GFP-tagged NMIIA. Only cells with clear filaments were chosen for the time lapse confocal microscopy. About 60 cells in 24 locations were monitored for over 24 h in each of 3 independent experiments. About 20-30% of monitored cells either died or were lost in the field of view before 24 h and were censored. About 50-60% of the remainder with GFP-IIA fluorescent filaments underwent a significant (Student's t test, P≤0.039) redistribution from an even to a more peripheral location upon induction of S100P (Fig. 5A)(Supplemental Table 3), the remaining 30-40% did not show obvious change in distribution of filaments. In contrast, when S100P was not induced in HeLa-A3, A19 cells or HeLa cells were treated with doxycycline, cells with fluorescent NMIIA containing filaments exhibited a similar low level of about 10% of peripherally distributed filaments (Supplemental Table 3). The amount of Triton-insoluble NMIIA was also significantly reduced by about 30-40% in HeLa-A19 cells 24 h after adding 1 μg/ml doxycycline compared to that without doxycycline (Figs. 5B&C)(P<0.05) but no significant difference between HeLa cells with or without doxycycline treatment. These data indicate that S100P-induced redistribution of NMIIA is companied by the dissociation of NMIIA filaments.

NMIIA peptide blocks NMIIA-S100P interaction and S100P-enhanced cell migration. The S100P binding domain of NMIIA (Fig. 6A) was fused with TAT-HA2 (38). TAT is the HIV Tat protein transduction domain and is used for delivery of peptides into cells (Fig. 6A) (49). Since TAT-delivered peptides are often trapped in macropinosomes, HA2, the *N*-terminal of the influenza virus hemagglutinin protein, a well characterized, pH-sensitive peptide that destabilizes lipid membranes at low pH (50), was also incorporated to assist the escape of trapped peptides and improve their cellular activity (38). The resultant fusion peptide specifically blocked the interaction of S100P with immobilised NMIIA (Fig. 6B) and the FITC-labelled peptide was taken up by cells after an overnight incubation (Fig. 6C). When the fusion peptide was pre-incubated with HeLa-A19 cells for 48 h, cell migration was significantly increased by nearly 40% (Fig. 6D). This is probably because the peptide also

partially overlaps the bundling domain of NMIIA (Figs. 2A, 6A)(46). Importantly, however, the peptide nearly completely inhibited the S100P-enhanced increase in cell migration (Fig. 6D). The control peptide containing only TAT-HA2 entered cells, but did not significantly affect cell migration with or without induction of S100P (Fig. 6D). These results support the contention that S100P targets NMIIA to enhance cell migration.

Effects of S100P upregulation and NMII knockdown on focal adhesion sites (FAS). When FAS were located by immunofluorescent staining for vinculin and by phalloidin staining actin filaments, the majority of actin filaments terminated at FAS in the HeLa cells (Figs. 7A&B). In parental HeLa and non-induced HeLa-A3 or A19 cells, FAS and actin filaments were evenly distributed (Figs. 7A-C) and only 5-10% of the fluorescent cells exhibited a peripheral distribution of FAS (Supplemental Table 4). When S100P was induced for 24 h, the number of FAS in the HeLa-A3 and A19 cells was significantly reduced by 2-3 fold ($P \leq 0.012$, Supplemental Table 5) producing a peripheral distribution in 40-50% of stained cells (Figs. 7E&F) (Supplemental Table 4). In parallel, actin filaments became more peripherally distributed than in HeLa (Fig. 7E&F) or in untreated cells (Figs. 7A-C). When NMIIA was knocked down in HeLa cells, FAS were reduced by 10-20 fold ($P=0.001$) (Supplemental Table 5), and virtually disappeared, but the fewer thicker actin filaments were not redistributed to the cellular peripheries (Fig. 7G). In contrast, when NMIIB (7H) and IIC (7I) were knocked down, there was no obvious effect on the average numbers/cell nor distribution of either FAS or actin filaments. These data suggest that S100P-induced NMIIA dissociation caused the redistribution and reduction of vinculin-containing and actin-terminating FAS.

Inhibition of vinculin production simulates S100P enhanced cell migration. Specific siRNAs to vinculin mRNA knocked down its protein level by about 80% (Fig.8A) and significantly increased HeLa –A19 cell migration by nearly 2-fold (Fig.8B). However, there was no further significant increase in cell migration upon induction of S100P (Fig.8B). Control siRNA not directed to vinculin mRNA was without any effect (Figs.8A, B). The vinculin-containing FAS in HeLa-A19 cells after knockdown of vinculin also became much less apparent (Fig.8C). These data demonstrate that S100P functions via a reduction in vinculin and FAS to increase cell migration.

Effects of S100P induction on cell adhesion. Both NMIIA filaments and their associated FAS are important for cell adhesion (51). The effect of S100P on both NMIIA and FAS will be eventually reflected by cell adhesion changes. When seeded on plastic surfaces the cellular adhesion of HeLa cells treated with doxycycline was not significantly different from that of untreated HeLa cells (Fig. 9A). Once HeLa–A19 cells were treated with doxycycline to induce S100P, cellular adhesion was significantly reduced by 30-50% at 60 and 90 min compared to that of non-induced HeLa-A19 cells (Student's t test $P \leq 0.02$)(Fig. 9B), indicating that induction of S100P is able to reduce significantly cell adhesion to plastic surfaces in tissue culture. Further analysis showed that induction of S100P significantly reduced cell adhesion to collagen I and II coated surfaces, but not to surfaces coated with collagen IV, fibronectin, laminin, tenascin or vitronectin (Figs. 9C&D). The reason for the differential effects is not clear.

Inhibition of FAK kinase abolishes the stimulatory effect of S100P on cell migration. To investigate whether cell migration stimulated by S100P in HeLa cells requires activation of focal adhesion kinase (FAK), the major kinase for assembly and disassembly of FAS (52,53), an inhibitor of its phosphorylation, TAE226 (54) was added 6 h after plating the cells in a Boyden Chamber. Addition of 0.5 to 5 μM TAE226 reduced cell migration in a dose-dependent manner in HeLa-A3 cells. S100P-enhanced cell migration was abolished when TAE226 concentration exceeded 1 μM (Fig. 10A), at which the FAK phosphorylation (Y397) was significantly inhibited (Supplemental Fig. 5). There was no significant effect on cell proliferation in the same time period (Fig. 10B) (ANOVA test, $P \geq 0.23$). Induction of S100P did not change the ratio of pFAK/FAK significantly (Supplemental Fig. 5). When S100P was induced in HeLa-A3 cells in the presence of TAE226, there was no significant reduction ($P=0.11$, Supplemental Table 6) nor significant peripheral redistribution of FAS ($P=0.09$) (Fig 10C panel F). However rearrangement of NMIIA was still observed ($P=0.01$) but in about only half of the cells compared to those without TAE226 ($P=0.03$)(Fig. 10C, panel C and Supplemental Table 6). These results suggest that S100P-enhanced cell migration requires functional FAK kinase and redistribution of FAS.

DISCUSSION

Migration of cancer cells away from the primary tumor is the critical initial step in metastasis (55,56). We have demonstrated previously that both S100A4 and S100P are able to promote metastasis in a syngeneic rat model for breast cancer and that their overexpression in human breast cancer specimens indicate a poor patient prognosis (4,7,10). In this work, we demonstrate that high levels of S100P are able to increase cell migration, both in S100P stably transfected and S100P inducible rat and human cell lines. Although it has been reported that S100A4 and other S100 proteins are associated with cell migration (57), this work is the first to establish a direct cause and effect relationship between levels of S100P and cell migration (linear regression, r=0.93, P=0.035) (Supplemental Fig. 3C).

The driving force for migration in non-muscle cells arises mainly from the acto-myosin filaments (58). Non-muscle myosin II (NMII) is able to form acto-myosin fibres in non-muscle cells and currently three isoforms have been identified. The NMIIA and IIB have opposite effects on cell migration with NMIIB serving as the driving force, whilst the NMIIA filaments serve mainly as a scaffold through which a cell adheres, through FAS, to the culture substratum, thereby anchoring it. How NMIIB drives cell migration is not entirely clear, but its involvement in cell polarisation and tail retraction (59) could enhance directional movement of cells. In our work, we confirm that knockdown of NMIIB reduces but knockdown of NMIIA enhances cell migration, knockdown of NMIIC shows no significant effect. More relevantly, only knockdown of NMIIA significantly affects S100P-enhanced cell migration, which suggests that NMIIA is the major effector of the S100P pathway. This point has been confirmed by both in vitro and in vivo studies. In vitro, we show S100P differentially interacts with the NMII isoforms with its highest affinity for NMIIA (>NMIIC>>NMIIB). Therefore, S100P mainly affects filament formation of NMIIA and NMIIC but not NMIIB, similar to that observed with S100A4 (12,60-64). With respect to the relationship of structure to function, a major site identified on NMIIA to which S100P binds *in vitro* (Fig.2A) is contained within a polypeptide of NMIIA that, when incorporated into HeLa-A19 cells, inhibits the ability of S100P to stimulate cell migration (Fig.6). In contrast the site in the very similar S100A4 to which NMIIA binds is probably not linear, but involves several different regions of the S100 molecule (61), all of which, when mutated, inhibit its effect in stimulating Rama 37 cell migration and metastasis (62-64) and results for S100P, at least for the *C*-terminal region are similar (65).

In vivo, we demonstrate that S100P is partially co-localised with NMII filaments and their physical interaction in living cells has been confirmed using FRET. The same mutations in S100A4 that prevent binding of this molecule to a fragment of NMIIA using an optical biosensor *in vitro,* also prevent FRET between suitably engineered, fluorescent-labelled S100A4 and NMIIA in living HeLa cells (64), confirming that interaction also does not occur using these mutants *in vivo.* More importantly, we have for the first time demonstrated that S100P facilitates the dissociation of NMIIA filaments in living cells. This point is also supported by the fact that the total amount of insoluble NMIIA filaments is reduced after S100P induction. In HeLa-A3 or A19 cells, the distribution of S100P is more central and NMIIA filaments are normally distributed more uniformly before rather than after induction of S100P. The high levels of S100P in the central region induce the redistribution of NMIIA filaments to the cellular peripheries and thus may weaken their anchoring force. Inhibition of S100P stimulation of migration by a specific peptide of NMIIA containing the S100P binding region demonstrates that interaction between S100P and NMIIA is required for this effect in living cells.

The fact that dissociation of NMIIA filaments increases cell migration has also been observed in other cell systems. When blebbistatin is used to inhibit NMIIA contraction, the migration of mouse hepatic stellate cells is accelerated (66). The S1943A mutation of NMIIA increases its ability to form filaments and concomitantly reduces migration of MDA-MB 231 cells, while the S1943D or S1943E mutation decreases its assembly and promotes cell migration (67,68). Rho and Rac kinases are profound regulators of the cytoskeleton and hence also influence cell migration (69). With Rac1, one of the important pathways is Rac1/CDC42/PAK (P21-Activated Kinase), which causes disassembly of stress fibres and FAS, and enhances cell migration (70). Another important pathway is Rac1/CDC42 /IQGAP1, which forms a complex that links the actin cytoskeleton and microtubules at the leading edges and facilitates cancer cell migration (71).

Thus , the Rac1 inhibitor, NSC23766 (72), which normally blocks dissociation of acto-myosin IIA filaments and FAS (73), inhibits migration of S100P- expressing HeLa-A3 cells (Supplemental Fig. 6A). Moreover, specific siRNAs to Rac1 knocked down over 90% of Rac1 protein in HeLa-A19 cells and significantly reduce cell migration by about 67% and 83%, respectively, and to the same basal rate in uninduced and S100P-induced cells (Supplemental Figs. 6B,C). Rac1 knockdown also caused abundant and abnormal NMIIA filaments (Supplemental Fig. 6D). With Rho activation, integrin clusters are aligned through their attachment to the ends of stress fibres to form FAS. Thus inhibition of Rho-ROCK activation by Y27623 (74), which normally blocks assembly of the acto-myosin IIA filaments and FAS formation (75,76), significantly increases cell migration in our cell systems. Similarly RhoA knockdown in HeLa-A19 cells by 70% using specific siRNAs reduced NMIIA filaments (Supplemental Figs.6C,D) and significantly enhanced cell migration by nearly 2-fold attaining the same rate as in S100P-induced cells; there was, however, no further increase in specific siRNA-treated S100P-induced cells (Supplemental Fig. 6B). These data strongly suggest that NMIIA filaments exert an anchoring rather than a migratory force. It appears that any mechanism that reduces NMIIA assembly, such as knockdown using specific siRNA, inhibition of Rho kinase and FAK or causes activation of Rac1 kinase and, as shown here, upregulation of certain S100 proteins will eventually facilitate cells to migrate away from their current location (Supplemental Fig.7)

In this study, we show that knockdown of NMIIA but not NMIIB or IIC dramatically reduces the number of vinculin-containing FAS, confirming reports in other cell systems (23,77). For example, when the contractility of acto-myosin is reduced by inhibition of myosin light chain phosphorylation or by blebbistatin, an inhibitor of myosin II, the FAS lose vinculin and talin and consequently reduce their adhesion forces (51). However, these methods of inhibiting contractility of acto-myosin do not change adhesion forces in vinculin null cells (51). These results suggest that NMIIA exerts its anchoring forces through talin and vinculin-containing FAS. FAS contains about 900 identified proteins and over half of them respond to the contractility changes of acto-myosin (78), indicating the fundamental influence of NMIIA on FAS. In our cell systems we show that the S100P-induced dissociation of NMIIA filaments is another means of reducing the number of vinculin-containing FAS.

The FAS is essential for cell adhesion (79). Here we show that induction of S100P significantly reduces the cell adhesion rates of HeLa-A19 cells, especially to surfaces coated with collagen I and II. This reduction in adhesion is most likely the consequence of the loss of FAS. One of the important modulators of the dynamic changes of FAS is FAK which also regulates the effects of NMIIA contractility on FAS (77,80). FAK signalling is critical to FAS turnover, therefore once FAS has been assembled, inhibition of FAK will prevent the loss of FAS (81). In our work, we show that TAE226, an inhibitor of FAK, significantly reduces the S100P-induced loss of FAS once it is added after cells adhere to culture surfaces. As a result, S100P-enhanced cell migration is also inhibited. Moreover inhibition of vinculin production by specific siRNAs both replicates and nullifies the stimulatory effect of S100P. Therefore this combined data suggests that S100P-enhanced cell migration also requires the disassembly of vinculin-containing FAS.

It is more than a decade since the interaction of S100A4 with a major motor protein NMIIA *in vitro* (12,20,82,83) and *in vivo* (37) has been identified, but it was not clear how this interaction (21) affects cell migration. Previous studies used S100A4 stable expression cells and its effects cannot be explicitly demonstrated. With the development of S100P-inducible cell lines, the dynamic changes of NMIIA filaments and associated FAS as well as cellular adhesion upon induction of S100P become much more obvious than that in stable expression cells and have been clearly demonstrated in this study. Accordingly, cell migration is much more strongly enhanced upon S100P induction than that in cells that stably express similar levels of S100P. These data suggest that oscillation of S100P in cancer cells may be more effective in promoting cell migration and metastasis. In summary, our new contribution here is the establishment of the direct cause-effect relationship between overexpression of S100P and cell migration as well as the underlying mechanism. This novel mechanism consists of a signal pathway involving dissociation of NMIIA filaments and a consequent weakening of FAS anchoring forces coupled with the unopposed locomotory action of unaffected NMIIB filaments to drive the cells forward. This work lays the

basis for why certain S100 proteins cause metastasis in rodent and human cancers.

REFERENCES

1. Heizmann, C. W., Fritz, G., and Schafer, B. W. (2002) *Front Biosci* **7**, d1356-1368
2. Donato, R. (2003) *Microsc Res Tech* **60**, 540-551.
3. Salama, I., Malone, P. S., Mihaimeed, F., and Jones, J. L. (2008) *Eur J Surg Oncol* **34**, 357-364
4. Rudland, P. S., Platt-Higgins, A., Renshaw, C., West, C. R., Winstanley, J. H., Robertson, L., and Barraclough, R. (2000) *Cancer Res* **60**, 1595-1603.
5. Helfman, D. M., Kim, E. J., Lukanidin, E., and Grigorian, M. (2005) *Br J Cancer* **92**, 1955-1958
6. Perez, D., Demartines, N., Meier, K., Clavien, P. A., Jungbluth, A., and Jaeger, D. (2007) *J Invest Surg* **20**, 181-186
7. Wang, G., Platt-Higgins, A., Carroll, J., de Silva Rudland, S., Winstanley, J., Barraclough, R., and Rudland, P. S. (2006) *Cancer Res* **66**, 1199-1207
8. Arumugam, T., Simeone, D. M., Van Golen, K., and Logsdon, C. D. (2005) *Clin Cancer Res* **11**, 5356-5364
9. Bronckart, Y., Decaestecker, C., Nagy, N., Harper, L., Schafer, B. W., Salmon, I., Pochet, R., Kiss, R., and Heizman, C. W. (2001) *Histol Histopathol* **16**, 707-712.
10. Davies, B. R., Davies, M. P., Gibbs, F. E., Barraclough, R., and Rudland, P. S. (1993) *Oncogene* **8**, 999-1008
11. Ford, H. L., Silver, D. L., Kachar, B., Sellers, J. R., and Zain, S. B. (1997) *Biochemistry* **36**, 16321-16327.
12. Kriajevska, M. V., Cardenas, M. N., Grigorian, M. S., Ambartsumian, N. S., Georgiev, G. P., and Lukanidin, E. M. (1994) *J Biol Chem* **269**, 19679-19682
13. Whiteman, H. J., Weeks, M. E., Dowen, S. E., Barry, S., Timms, J. F., Lemoine, N. R., and Crnogorac-Jurcevic, T. (2007) *Cancer Res* **67**, 8633-8642
14. Conti, M. A., Even-Ram, S., Liu, C., Yamada, K. M., and Adelstein, R. S. (2004) *J Biol Chem* **279**, 41263-41266
15. Lo, C. M., Buxton, D. B., Chua, G. C., Dembo, M., Adelstein, R. S., and Wang, Y. L. (2004) *Mol Biol Cell* **15**, 982-989
16. Tullio, A. N., Accili, D., Ferrans, V. J., Yu, Z. X., Takeda, K., Grinberg, A., Westphal, H., Preston, Y. A., and Adelstein, R. S. (1997) *Proc Natl Acad Sci U S A* **94**, 12407-12412.
17. Uren, D., Hwang, H. K., Hara, Y., Takeda, K., Kawamoto, S., Tullio, A. N., Yu, Z. X., Ferrans, V. J., Tresser, N., Grinberg, A., Preston, Y. A., and Adelstein, R. S. (2000) *J Clin Invest* **105**, 663-671.
18. Golomb, E., Ma, X., Jana, S. S., Preston, Y. A., Kawamoto, S., Shoham, N. G., Goldin, E., Conti, M. A., Sellers, J. R., and Adelstein, R. S. (2004) *J Biol Chem* **279**, 2800-2808
19. Wylie, S. R., and Chantler, P. D. (2008) *Mol Biol Cell* **19**, 3956-3968
20. Kriajevska, M., Tarabykina, S., Bronstein, I., Maitland, N., Lomonosov, M., Hansen, K., Georgiev, G., and Lukanidin, E. (1998) *J Biol Chem* **273**, 9852-9856
21. Li, Z. H., and Bresnick, A. R. (2006) *Cancer Res* **66**, 5173-5180
22. Li, Z. H., Spektor, A., Varlamova, O., and Bresnick, A. R. (2003) *Biochemistry* **42**, 14258-14266
23. Even-Ram, S., Doyle, A. D., Conti, M. A., Matsumoto, K., Adelstein, R. S., and Yamada, K. M. (2007) *Nat Cell Biol* **9**, 299-309
24. Wang, G., Rudland, P. S., White, M. R., and Barraclough, R. (2000) *J Biol Chem* **275**, 11141-11146
25. Lamartina, S., Silvi, L., Roscilli, G., Casimiro, D., Simon, A. J., Davies, M. E., Shiver, J. W., Rinaudo, C. D., Zampaglione, I., Fattori, E., Colloca, S., Gonzalez Paz, O., Laufer, R., Bujard, H., Cortese, R., Ciliberto, G., and Toniatti, C. (2003) *Mol Ther* **7**, 271-280
26. Albini, A., Iwamoto, Y., Kleinman, H. K., Martin, G. R., Aaronson, S. A., Kozlowski, J. M., and McEwan, R. N. (1987) *Cancer Res* **47**, 3239-3245

27. Wang, G., Zhang, S., Fernig, D. G., Martin-Fernandez, M., Rudland, P. S., and Barraclough, R. (2005) *Oncogene* **24**, 1445-1454.
28. Wang, G., Zhang, S., Fernig, D. G., Spiller, D., Martin-Fernandez, M., Zhang, H., Ding, Y., Rao, Z., Rudland, P. S., and Barraclough, R. (2004) *Biochem J* **382**, 375-383
29. Gibbs, F. E., Wilkinson, M. C., Rudland, P. S., and Barraclough, R. (1994) *J Biol Chem* **269**, 18992-18999
30. Chen, H., Fernig, D. G., Rudland, P. S., Sparks, A., Wilkinson, M. C., and Barraclough, R. (2001) *Biochem Biophys Res Commun* **286**, 1212-1217
31. Ho, S. N., Hunt, H. D., Horton, R.M., Pullen, J. K., and Please, L. R. (1989) *Gene* **77**, 51-59
32. Wang, G., Ma, A., Chow, C. M., Horsley, D., Brown, N. R., Cowell, I. G., and Singh, P. B. (2000) *Mol Cell Biol* **20**, 6970-6983.
33. Laemmli, U. K. (1970) *Nature* **227**, 680-685
34. Fernig, D. G. (2001) *Methods Mol. Biol.* **171**, 505-518
35. Murakami, N., Singh, S. S., Chauhan, V. P., and Elzinga, M. (1995) *Biochemistry* **34**, 16046-16055
36. Pepperkok, R., Squire, A., Geley, S., and Bastiaens, P. I. H. (1999) *Current Biol.* **9**, 269-272
37. Zhang, S., Wang, G., Fernig, D. G., Rudland, P. S., Webb, S. E., Barraclough, R., and Martin-Fernandez, M. (2005) *Eur Biophys J* **34**, 19-27
38. Wadia, J. S., Stan, R. V., and Dowdy, S. F. (2004) *Nat Med* **10**, 310-315
39. Humphries, M. J. (2009) *Methods Mol Biol* **522**, 203-210
40. Arumugam, T., Ramachandran, V., and Logsdon, C. D. (2006) *J Natl Cancer Inst* **98**, 1806-1818
41. Fuentes, M. K., Nigavekar, S. S., Arumugam, T., Logsdon, C. D., Schmidt, A. M., Park, J. C., and Huang, E. H. (2007) *Dis Colon Rectum* **50**, 1230-1240
42. Donato, R. (2007) *Curr Mol Med* **7**, 711-724
43. Arumugam, T., Simeone, D. M., Schmidt, A. M., and Logsdon, C. D. (2004) *J Biol Chem* **279**, 5059-5065.
44. Vallely, K. M., Rustandi, R. R., Ellis, K. C., Varlamova, O., Bresnick, A. R., and Weber, D. J. (2002) *Biochemistry* **41**, 12670-12680
45. Zhang, H., Wang, G., Ding, Y., Wang, Z., Barraclough, R., Rudland, P. S., Fernig, D. G., and Rao, Z. (2003) *J Mol Biol* **325**, 785-794
46. Dulyaninova, N. G., Malashkevich, V. N., Almo, S. C., and Bresnick, A. R. (2005) *Biochemistry* **44**, 6867-6876
47. Bastiaens, P. I., and Squire, A. (1999) *Trends Cell Biol* **9**, 48-52
48. Elangovan, M., Day, R. N., and Periasamy, A. (2002) *J Microsc* **205**, 3-14
49. Schwarze, S. R., Ho, A., Vocero-Akbani, A., and Dowdy, S. F. (1999) *Science* **285**, 1569-1572
50. Han, X., Bushweller, J. H., Cafiso, D. S., and Tamm, L. K. (2001) *Nat Struct Biol* **8**, 715-720
51. Dumbauld, D. W., Shin, H., Gallant, N. D., Michael, K. E., Radhakrishna, H., and Garcia, A. J. (2010) *J Cell Physiol* **223**, 746-756
52. Sieg, D. J., Hauck, C. R., and Schlaepfer, D. D. (1999) *J Cell Sci* **112 (Pt 16)**, 2677-2691
53. Gilmore, A. P., and Romer, L. H. (1996) *Mol Biol Cell* **7**, 1209-1224
54. Wang, Z. G., Fukazawa, T., Nishikawa, T., Watanabe, N., Sakurama, K., Motoki, T., Takaoka, M., Hatakeyama, S., Omori, O., Ohara, T., Tanabe, S., Fujiwara, Y., Shirakawa, Y., Yamatsuji, T., Tanaka, N., and Naomoto, Y. (2008) *Oncol Rep* **20**, 1473-1477
55. Cairns, R. A., Khokha, R., and Hill, R. P. (2003) *Curr Mol Med* **3**, 659-671.
56. Hirohashi, S. (1998) *Am J Pathol* **153**, 333-339.
57. Jenkinson, S. R., Barraclough, R., West, C. R., and Rudland, P. S. (2004) *Br J Cancer* **90**, 253-262.
58. Vicente-Manzanares, M., Ma, X., Adelstein, R. S., and Horwitz, A. R. (2009) *Nat Rev Mol Cell Biol* **10**, 778-790
59. Swailes, N. T., Colegrave, M., Knight, P. J., and Peckham, M. (2006) *J Cell Sci* **119**, 3561-3570
60. Badyal, S. K., Basran, J., Bhanji, N., Kim, J. H., Chavda, A. P., Jung, H. S., Craig, R., Elliott, P. R., Irvine, A. F., Barsukov, I. L., Kriajevska, M., and Bagshaw, C. R. (2011) *J Mol Biol* **405**, 1004-1026

61. Li, Z. H., Dulyaninova, N. G., House, R. P., Almo, S. C., and Bresnick, A. R. (2010) *Mol Biol Cell* **21**, 2598-2610
62. Ismail, T. M., Fernig, D. G., Rudland, P. S., Terry, C. J., Wang, G., and Barraclough, R. (2008) *Carcinogenesis* **29**, 2259-2266
63. Ismail, T. M., Zhang, S., Fernig, D. G., Gross, S., Martin-Fernandez, M. L., See, V., Tozawa, K., Tynan, C. J., Wang, G., Wilkinson, M. C., Rudland, P. S., and Barraclough, R. (2010) *J Biol Chem* **285**, 914-922
64. Zhang, S., Wang, G., Liu, D., Bao, Z., Fernig, D. G., Rudland, P. S., and Barraclough, R. (2005) *Oncogene* **24**, 4401-4411
65. Ismail, T. M., Gross, S., Goh, C., Wilkinson, M. C., Rudland, P. S., and Barraclough, R. (2011) The C-terminal amino acids of S100A4 and S100P play a role in cell migration and metastasis. in *Montreal International Symposium on Angiogenesis and Metastasis*, Montreal, Canada, p101.
66. Liu, Z., van Grunsven, L. A., Van Rossen, E., Schroyen, B., Timmermans, J. P., Geerts, A., and Reynaert, H. (2010) *Br J Pharmacol* **159**, 304-315
67. Dulyaninova, N. G., House, R. P., Betapudi, V., and Bresnick, A. R. (2007) *Mol Biol Cell* **18**, 3144-3155
68. Breckenridge, M. T., Dulyaninova, N. G., and Egelhoff, T. T. (2009) *Mol Biol Cell* **20**, 338-347
69. Burridge, K., and Wennerberg, K. (2004) *Cell* **116**, 167-179
70. Dummler, B., Ohshiro, K., Kumar, R., and Field, J. (2009) *Cancer Metastasis Rev* **28**, 51-63
71. Watanabe, T., Noritake, J., and Kaibuchi, K. (2005) *Novartis Found Symp* **269**, 92-101; discussion 101-105, 223-130
72. Noritake, J., Watanabe, T., Sato, K., Wang, S., and Kaibuchi, K. (2005) *J Cell Sci* **118**, 2085-2092
73. Manser, E., Huang, H. Y., Loo, T. H., Chen, X. Q., Dong, J. M., Leung, T., and Lim, L. (1997) *Mol Cell Biol* **17**, 1129-1143
74. Darenfed, H., Dayanandan, B., Zhang, T., Hsieh, S. H., Fournier, A. E., and Mandato, C. A. (2007) *Cell Motil Cytoskeleton* **64**, 97-109
75. Sandquist, J. C., Swenson, K. I., Demali, K. A., Burridge, K., and Means, A. R. (2006) *J Biol Chem* **281**, 35873-35883
76. Anderson, S., DiCesare, L., Tan, I., Leung, T., and SundarRaj, N. (2004) *Exp Cell Res* **298**, 574-583
77. Pasapera, A. M., Schneider, I. C., Rericha, E., Schlaepfer, D. D., and Waterman, C. M. (2010) *J Cell Biol* **188**, 877-890
78. Kuo, J. C., Han, X., Hsiao, C. T., Yates Iii, J. R., and Waterman, C. M. (2011) *Nat Cell Biol* **13**, 383-393
79. Berrier, A. L., and Yamada, K. M. (2007) *J Cell Physiol* **213**, 565-573
80. Ilic, D., Furuta, Y., Kanazawa, S., Takeda, N., Sobue, K., Nakatsuji, N., Nomura, S., Fujimoto, J., Okada, M., and Yamamoto, T. (1995) *Nature* **377**, 539-544
81. Ren, X. D., Kiosses, W. B., Sieg, D. J., Otey, C. A., Schlaepfer, D. D., and Schwartz, M. A. (2000) *J Cell Sci* **113 (Pt 20)**, 3673-3678
82. Ford, H. L., and Zain, S. B. (1995) *Oncogene* **10**, 1597-1605
83. Kriajevska, M., Bronstein, I. B., Scott, D. J., Tarabykina, S., Fischer-Larsen, M., Issinger, O., and Lukanidin, E. (2000) *Biochim Biophys Acta* **1498**, 252-263

FOOTNOTES

This work was supported by the Cancer and Polio Research Fund and the North West Cancer Research Fund. Thanks to Dr.Marisa Martin-Ferandez for overseeing the FRET experiments and analysis at the Synchrotron Radiation Facility at Daresbury, Cheshire. UK.
The abbreviations used are: CFP, cyan fluorescent protein; HRP: horse radish peroxidase; PKC: protein kinase C; NMII: non-muscle myosin II. FAS: focal adhesion sites; FAK: focal adhesion kinase; GFP: green fluorescent protein; RAGE: receptor for advanced glycation endproducts; siRNA: small interference RNA; YFP: yellow fluorescent protein.

TABLES

Table 1. Kinetics of binding of soluble S100P to immobilised r*C*-NMII isoforms

Immobilised Protein	k_{ass} ($M^{-1}s^{-1}$)[a] Mean ± S.E.	R[b]	K_{diss} (s^{-1})[c] Mean ± S.E.	K_d (nM)[d] (kinetic) Mean ± S.E.	K_d (nM)[e] (equilibrium) Mean ± S.E.
rC-NMIIA	8900 ±2400	0.91-0.98	0.0039±0.0007	430±210	500±200
rC-NMIIB	990±350	0.94-0.96	0.0078±0.0031	7800±4200	8400±1200
rC-NMIIC	6800±3300	0.82-0.95	0.0068±0.0016	1000±530	490±100

[a] The S.E. of each determination of k_{ass} is derived from the deviation of 4 independent data sets from a one-site binding model, calculated by matrix inversion using the FastFit software provided with the instrument (Experimental Procedures). No evidence was found for a two-site model of association.

[b] The correlation coefficient of the linear regression through the k_{on} values used for obtaining k_{ass}.

[c] The k_{diss} is the mean ± S.E. of 7 values, obtained at different concentrations of S100P. No evidence was found for a two-site model of dissociation.

[d] The K_d (kinetic) was calculated from the ratio of k_{diss}/k_{ass}, and the S.E. is the combined S.E. of the two kinetic parameters.

[e] The K_d (equilibrium) was calculated from the extent of binding observed at or near equilibrium at 6 or more different concentrations of S100P in 4 independent experiments. The S.E. is the combined error of the 4 experiments.

FIGURE LEGENDS

Fig. 1. Effect of S100P on cell migration. Representative examples of the corresponding Western blot of S100P and actin from Rama 37 cells (A) transfected with control vector (lane 1) and S100P expression vector (lane 2, pool 1; lane 3, pool 2; lane 4, isolated clone 1 and lane 5, isolated clone 2) and from MCF-7 cells (C) transfected with control siRNA (lane 1), S100P specific siRNA-1 and 2 (lanes 2 and 3) for 48 h. Mean ±SD percentages of corresponding changes of cell migration of transfected Rama 37 cells in 24 h (B) or transfected MCF-7 cells in 72 h (D) are shown. *Significantly increased in ANOVA test, $P<0.01$. (E) A representative example of Western blots shows the relative levels of S100P after induction of R37-T25, T28 and HeLa-A3, A19 cells with 1 µg/ml of doxycycline for 24 h. (F) Mean ±SD percentages of cell migration in 24 h after induction with doxycycline relative to those before induction (the control migrations are set at 100%). *Significantly increased in Student's t test $p \leq 0.008$ when compared before and after doxycycline induction. (G) R37-T25 and HeLa -A3 cells were cultured in medium without FCS, but supplemented with 1 mg/ml of bovine albumin with or without doxycycline (1 µg/ml) for 48 h. One ml of medium with doxycycline from each cell line was collected and freeze dried. S100P was detected by Western blotting. (H) Effect of inhibiting RAGE receptor on cell migration of R37-T25 (■) and HeLa-A3 cells (□). Cells were treated without (Control) or with 1 µg/ml doxycycline (Doxy), 100 nM rhS100P, 5 µg/ml anti-RAGE antibody (R&D, Abingdon, UK) or 500 nM amphoterin-derived peptide (peptide) (Sigma, Gillingham, UK). Cell migration of untreated cells (Control) was set to 100%. Doxycycline alone or with anti-RAGE antibody and amphoterin-derived peptide all significantly increased cell migration, * (Student's t test, $P \leq 0.031$ compared to control). Treatments with rhS100P showed no significant differences ($P \geq 0.2$ compared with controls). Anti-RAGE antibody and amphoterin-derived peptide did not significantly reduce S100P-enhanced cell migration (Student's t test, $P \geq 0.18$ compared with doxy alone).

Fig. 2. Interaction of S100P with NMIIA and its effects on the formation of filaments (A) Amino acid sequence alignment of the tail region of the three NMII isoforms; the bundling domain (IIA, 1855-1903) and a major S100P-binding site (IIA, 1909-1937) are indicated. (B) Diagram of NMIIA mutations generated. (C) Gel overlay assay with S100P (upper panel) and S100A4 (middle panel) protein to show their interaction with deletion mutants (M1, M2, M3, M4, and M5) and wild type (WT) NMIIA *C*-terminal fragments (Experimental Procedures). Lower panel shows the Coomassie blue-stained gel of mutant and wt NMIIA *C*-terminal fragments used for the gel overlay assay. (D) Examples of Western blotting with anti-histag antibody to soluble polyhistidine-tagged NMIIs *C*-terminal fragments to demonstrate the effect of different concentrations of S100P on formation of NMII filaments *in vitro*. B=Sample taken before filament formed. The remaining lanes are the same volume of samples taken from the supernatants after precipitation of NMII filaments by centrifugation. (E) The mean ±SD in arbitrary units of quantified non-filament NMIIs in the supernatant plotted against µM of S100P from three independent experiments for IIA ( ), IIB (■) and IIC (▲). (F) Bundling buffer containing 0 and 3 µM S100P was used to resuspend the filaments that formed with 0 S100P as shown in (E). After 40 min incubation, the resuspended filaments were centrifuged and the rest of the procedures were the same as those in (D) above. (G) Mean arbitrary units of soluble NMII peptides from 3 independent experiments ±SD in (C) above were presented for control (■) and addition of 3 µM S100P (□). *Significant increase in Student's t test, $P \leq 0.007$).

Fig. 3. Effects of knocking down NMII isoforms and S100P induction on HeLa-A3 cell migration. Panels A-C: Effects of knockdown of NMII isoforms on cell migration after induction of S100P. HeLa-A3 cells were cultured without (*non-induced*, S100P was absent) or with (*induced*, S100P was present during siRNA knocking down and migration assay) doxycycline (1 µg/ml) 24 h before transfection with: control siRNA (■), specific siRNA-1 (□) or 2 (▨) to knock down NMIIA (A), IIB (B) and IIC (C). Cell migration was measured from 48 h to 72 h after transfection. Migration for control siRNA transfected cells is set at 100%. *ANOVA test, $P<0.05$ when compared to HeLa-A3 transfected with control siRNAs from at least 3 independent experiments. Panels D-F: Effects of induction of S100P on cell migration after knockdown of NMII isoforms. HeLa-A3 cells were cultured in medium without doxycycline for 24 h before transfection with specific siRNA-1 or 2 for

NMIIA (D), NMIIB (E) and NMIIC (F) or control siRNA (F). Cell migration was measured from 48 h to 72 h after transfection with (□) or without (■) 1 μg/ml doxycycline to induce S100P during migration assay. Migration for non-induced cells is set to 100%. *Significant increase observed in Student's t test P≤ 0.033 between cell migration with and without induction of S100P from at least 3 independent experiments.

Fig. 4. Co-localisation and physical interaction of S100P with NMIIA in living cells. (A) Dual immunofluorescent staining of MCF-7 cells with anti-S100P (Panels A, C) (green) and anti-NMIIA (panels B, C)(red) to demonstrate their co-localisation pattern (C, F). Panels D-F are the enlarged images of panels A-C, respectively. Arrows indicate some nodules where NMIIA and S100P co-localise. Bars=20 μm in A-C, and = 10 μm in D-F. (B) Fluorescence lifetime imaging of the interaction between S100P and NMIIA. Variations of the fluorescence lifetime distributions found in 5-7 different HeLa cells co-transfected with wild type ECFP-S100P + NMIIA-EYFP (Panel A) or ECFP-S100P + EYFP expression plasmids (B) as a control and their averages are shown in *panel C*.

Fig. 5. Dynamic changes of NMIIA in HeLa-A3 cells upon induction of S100P. (A) HeLa-A3 cells were transfected with plasmid to express GFP-NMIIA. After 16 h, doxycycline (1 μg/ml) was added to induce S100P, 24 microscopic fields covering about 60 cells with clear fluorescent fibres were selected and monitored (Experimental Procedures). Typical images at 0, 12, 18 and 24 h after addition of doxycycline are shown for the same cells. Bar=20 μm. (B) An example of Western blots of Triton-insoluble NMIIA from HeLa and HeLa-A19 cells with or without doxycycline treatment. Soluble actin serves as a loading control. (C) The mean±SD of the relative NMIIA/actin ratios from 3 independent experiments are presented by setting the ratio of NMIIA/actin from cells without doxycycline treatment as 100%. * Student's t test P<0.05.

Fig.6. Effects of NMIIA peptide on S100P-enhanced cell migration. (A) Amino acid sequence of target and control peptides. (B) Biosensor assay. 1 μM S100P was applied to NMIIA biosensor surface before (blue) or after blocking with 1 μM NMIIA peptide (green) or control peptide (red). (C) Images of HeLa-A19 cells. Target and control peptides were labelled with FITC (Sigma) and incubated with HeLa-A19 cells. Cells after 18 h with FITC-target peptides were fixed and stained with Atto-647N-phalloidin (Sigma). Images were recorded using a LSM5-10 confocal microscope. Both FITC-labelled control and NMIIA peptides were taken up by the cells. Only the typical images of FITC-NMIIA peptide are shown. Panel A, green dots indicate the FITC-NMIIA peptide taken up by cells and panel B, red filaments indicate the acto-myosin fibres, panel C is the transmission image and panel D is the superimposed image of A, B and C. (D) Cell migration assay was set up after 24 h incubation without (control) or with 5 μM non-labelled peptides in the presence or absence of doxycycline (1 μg/ml). Means±SD of relative migration rates to control are presented. * Student's t test, P<0.05 when compared to non-induced cells with the same treatment. **ANOVA test, P<0.05 when control/S100P-induced, NMIIA peptide-treated/S100P-induced cells, and control peptide-treated/induced cells are compared. ǂANOVA test, P<0.05 when non-induced cells with different treatments are compared.

Fig. 7. Dual fluorescent staining of actin filaments and FAS. HeLa (A, D), HeLa-A3 (B, E) and A19 cells (C, F) without (A-C, Control) or with (D-F, Doxy) induction of S100P by doxycycline for 24 h and HeLa cells with NMII isoforms knocked down using IIA siRNA-1(G), IIB siRNA-2 (H) and IIC siRNA-2 (I) were fixed and stained. Typical images of actin filaments (red) labelled by Atto 647N-Phalloidin (Sigma), FAS (green) located by fluorescently labelled vinculin (anti-vinculin, Sigma), and nuclei labelled with DAPI (blue) are shown. All bars=20 μm.

Fig. 8. Effects of knockdown of vinculin on cell migration. siRNAs specific for vinculin and control siRNA from Qiagen were transfected into HeLa-A19 cells. After 48 h, the cell migration assay was set up in the presence or absence of doxycycline. The rest of the cells were grown for further 24 h to check vinculin protein by Western blotting and immunofluorescent staining using anti-vinculin antibody. (A) Typical Western blot. (B) Means±SD of cell migration rates relative to control are shown. * Student's t test, P<0.05 compared between S100P non-induced and induced cells and P=0.61 compared between vinculin siRNA-treated, uninduced and S100P induced cells. **ANOVA test,

P=0.45 when control/S100P-induced, vinculin siRNA-treated/induced, and control siRNA-treated/induced cells are compared. ǂANOVA test, P<0.05 when uninduced cells with different treatments are compared. (C) Typical images of HeLa-A19 cells 72 h after transfection with control siRNA (panels A-C) and vinculin siRNA (panels D-F). Green dots indicate vinculin (panels A and D) and red fibres indicate NMIIA (panels B and E). Panels C and F are the superimposed images of panels A and B, and panels D and E, respectively. Bars = 20 μm.

Fig. 9. Effect of S100P on cell adhesion**.** HeLa (A) and HeLa-A19 (B) were treated with (□) or without (■) doxycycline for 24 hours and cell adhesion assays were carried out as described in Experimental Procedures. The percentage of adhesion = 100 x cells retained on the surface of normal culture plate (Costar) /total cells seeded. The means±SD from 3 independent experiments were presented. The cell adhesion array kit (Millipore) was also used to detect the effect of S100P induction on the adhesion of HeLa (C) and HeLa-A19 (D) cells to surfaces coated with different extracellular matrix proteins. The cell adhesion without doxycycline treatment (■) was set as 100% and the means ±SD of relative adhesion after doxycycline treatment (□) are presented. * Student's t test, P≤0.02.

Fig. 10. Effect of FAK kinase inhibitor on cell migration and distribution of FAS. (A) Cell migration assay for HeLa –A3 cells with (□) or without (■) doxycycline (1μg/ml) and different concentrations of TAE226. The inhibitor was added 6 h after plating of the cells in the migration assay to allow them to adhere. After a further 18 h incubation, the cells were fixed and stained for counting and calculating the migration in 24 h (Experimental Procedures). Results are the mean±SD of 3 experiments. *Significant increase in Student's t test, p≤0.011 when comparing cell migration with (□) and without (■) doxycycline. (B) The inhibitor was added 6 h after 15,000 cells were plated in each well of a 24-well culture plate in medium containing 2% (v/v) FCS as in the migration assay. The cells were counted after a further 18 h incubation in the absence of doxycycline and the results are the mean ± SD of 3 experiments. (C) Dual immunofluorescent staining of NMIIA (red) (panels A-C) and FAS (green, vinculin) (panels D-F, same fields as A-C) in HeLa-A3 cells; (panels A, D) untreated cells; (panels B, E) cells treated with 1 μg/ml of doxycycline; and (panels C, F) cells treated with doxycycline plus 5 μM TAE226. Typical images are shown. All bars=50 μm.

Figure1

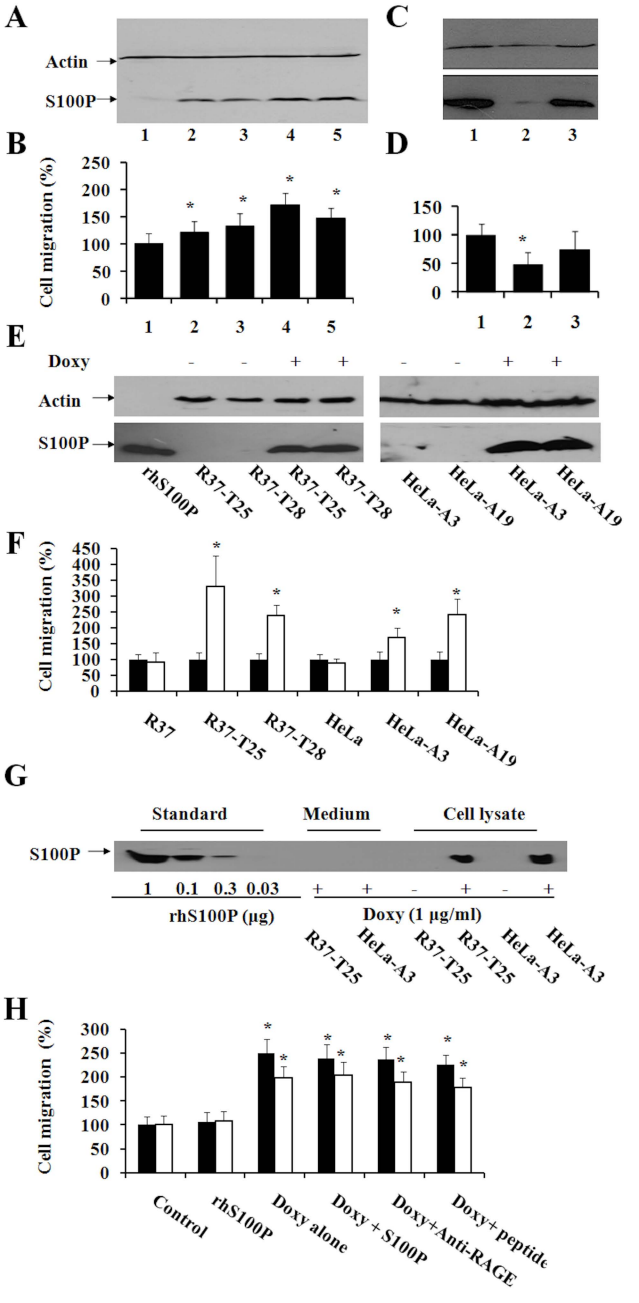
A
Actin
S100P
1 2 3 4 5
C
1 2 3
B
Cell migration (%)
250
200
150
100
50
0
1 2 3 4 5
D
150
100
50
0
1 2 3
E
Doxy - - + + - - + +
Actin
S100P
rhS100P
R37-T25
R37-T28
R37-T25
R37-T28
HeLa-A3
HeLa-A19
HeLa-A3
HeLa-A19
F
Cell migration (%)
450
400
350
300
250
200
150
100
50
0
R37
R37-T25
R37-T28
HeLa
HeLa-A3
HeLa-A19
G
Standard
Medium
Cell lysate
S100P
1 0.1 0.3 0.03
rhS100P (μg)
+ + - + - +
Doxy (1 μg/ml)
R37-T25
HeLa-A3
R37-T25
R37-T25
HeLa-A3
HeLa-A3
H
Cell migration (%)
300
250
200
150
100
50
0
Control
rhS100P
Doxy alone
Doxy + S100P
Doxy+Anti-RAGE
Doxy+peptide

Figure 2

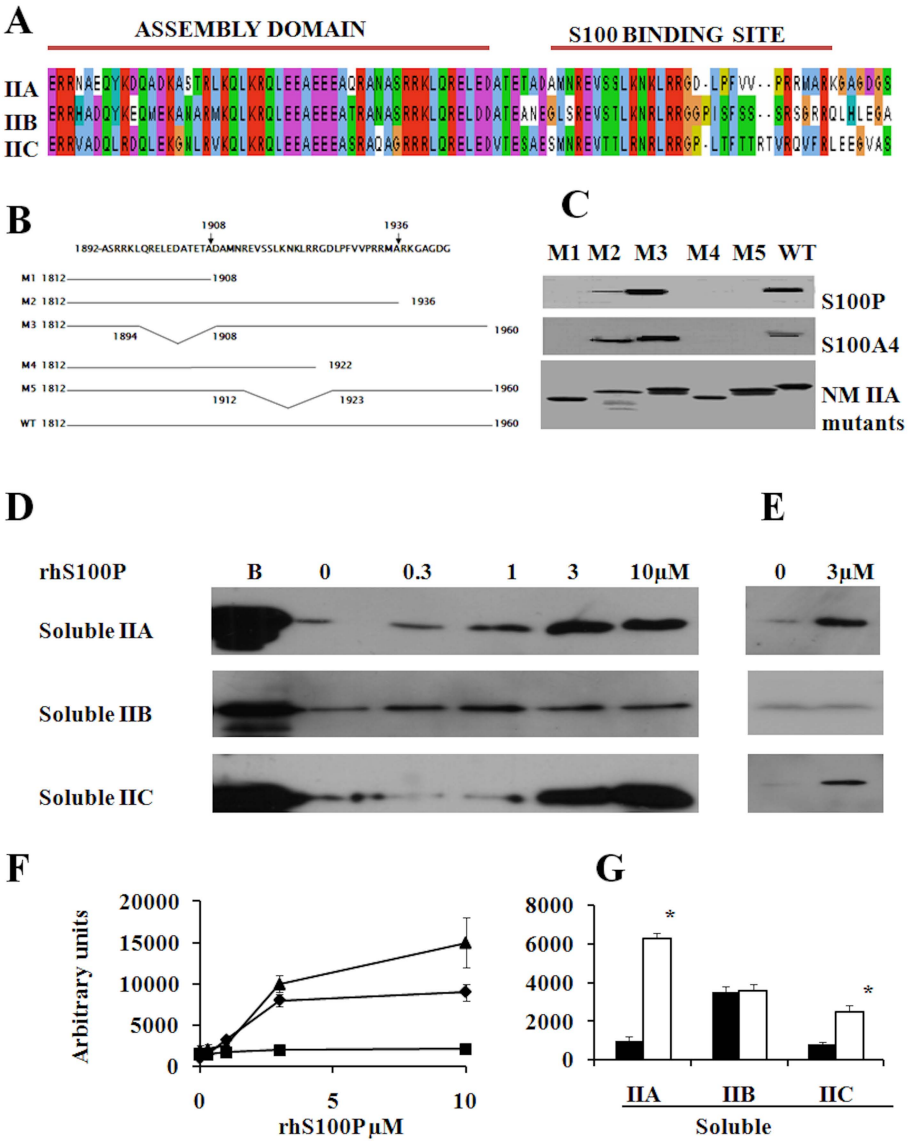
A
ASSEMBLY DOMAIN
S100 BINDING SITE
IIA
IIB
IIC
B
1908
1936
1892-ASRRKLQRELEDATETADAMNREVSSLKNKLRRGDLPFVVPRRMARKGAGDG
M1 1812 1908
M2 1812 1936
M3 1812 1894 1908 1960
M4 1812 1922
M5 1812 1912 1923 1960
WT 1812 1960
C
M1 M2 M3 M4 M5 WT
S100P
S100A4
NM IIA mutants
D
rhS100P
B 0 0.3 1 3 10µM
Soluble IIA
Soluble IIB
Soluble IIC
E
0 3µM
F
Arbitrary units
20000
15000
10000
5000
0
0 5 10
rhS100P µM
G
8000
6000
4000
2000
0
IIA IIB IIC
Soluble

Figure 3

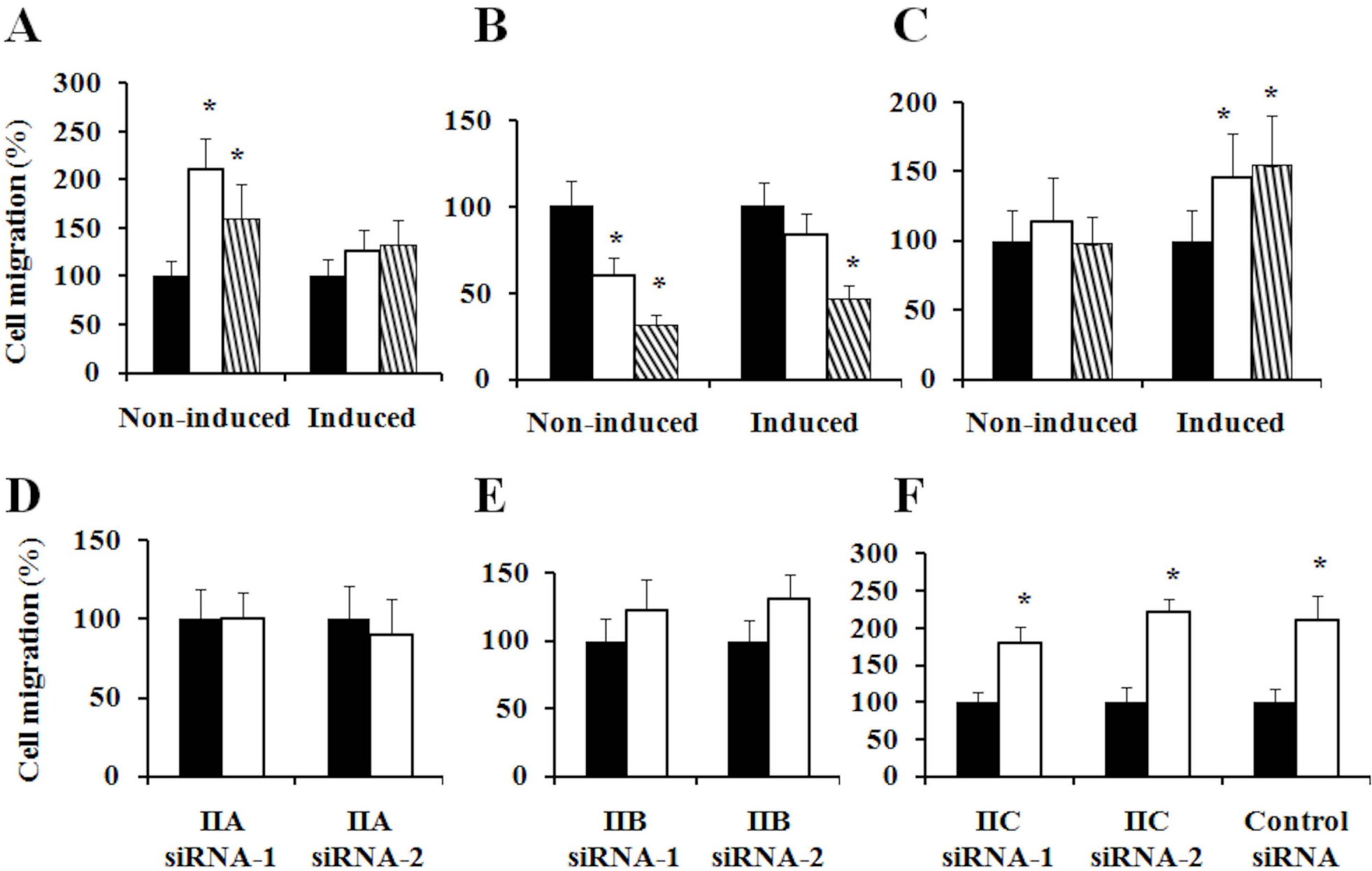
A
B
C
Cell migration (%)
300
250
200
150
100
50
0
*
Non-induced
Induced
150
100
50
0
200
150
100
50
0
D
E
F
IIA siRNA-1
IIA siRNA-2
IIB siRNA-1
IIB siRNA-2
IIC siRNA-1
IIC siRNA-2
Control siRNA

Figure 4

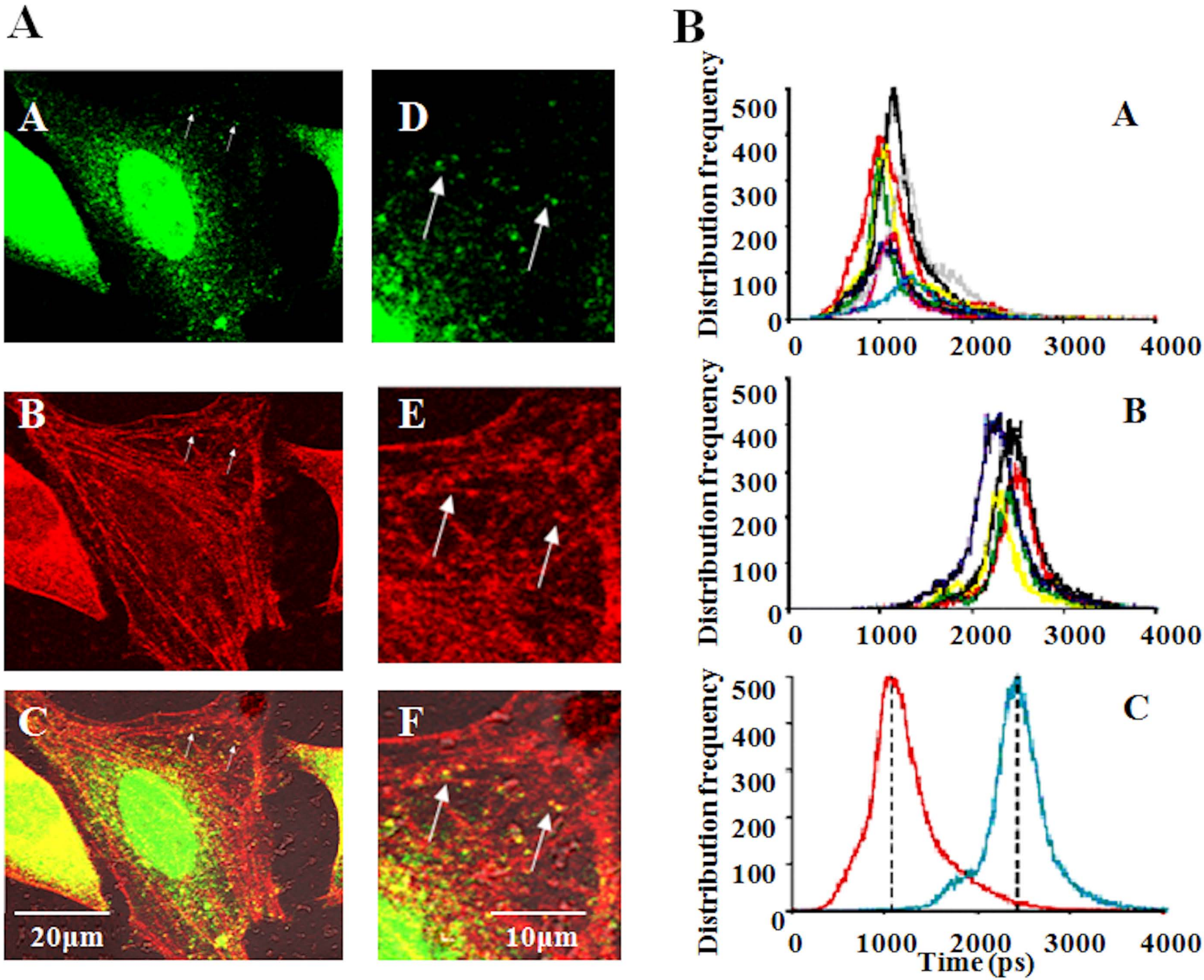
A
A
D
B
E
C
F
20μm
10μm
B
Distribution frequency
500
400
300
200
100
0
0
1000
2000
3000
4000
A
B
C
Time (ps)

Figure 5

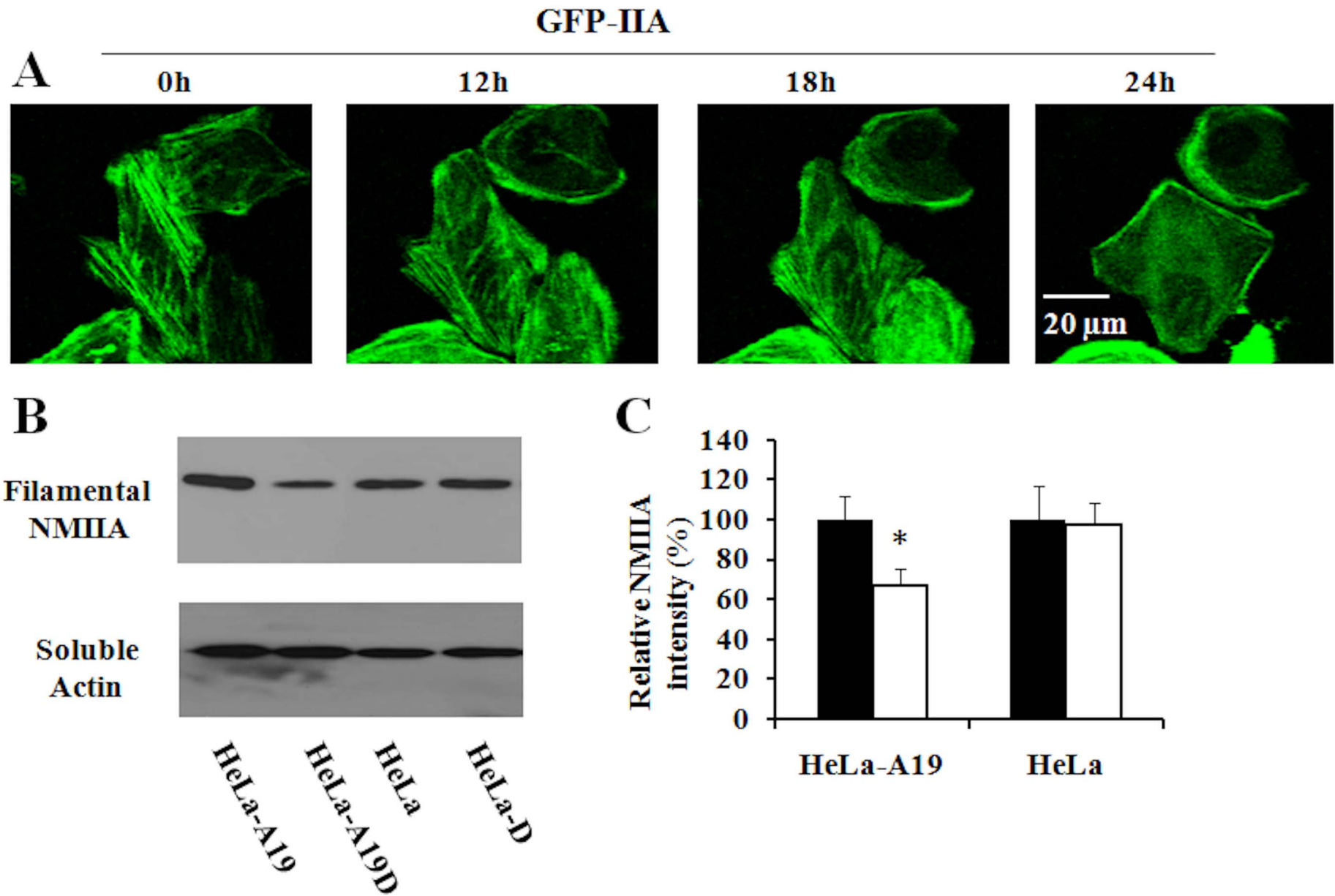
GFP-IIA
A
0h
12h
18h
24h
20 μm
B
Filamental NMIIA
Soluble Actin
HeLa-A19
HeLa-A19D
HeLa
HeLa-D
C
Relative NMIIA intensity (%)
140
120
100
80
60
40
20
0
*
HeLa-A19
HeLa

Figure 6

A

HA2-TAT-NMIIA motif peptide

GDIMGEWGNEIFGAIAGFLG (HA2) -
RRRQRRKKRG (TAT) -
QRELEDATETADAMNREVSSLKNKLRRGDL
PFVVPRRMA (NMIIA S100 binding domain)

HA2-TAT control peptide

GDIMGEWGNEIFGAIAGFLG (HA2) -
RRRQRRKKRG (TAT)

B

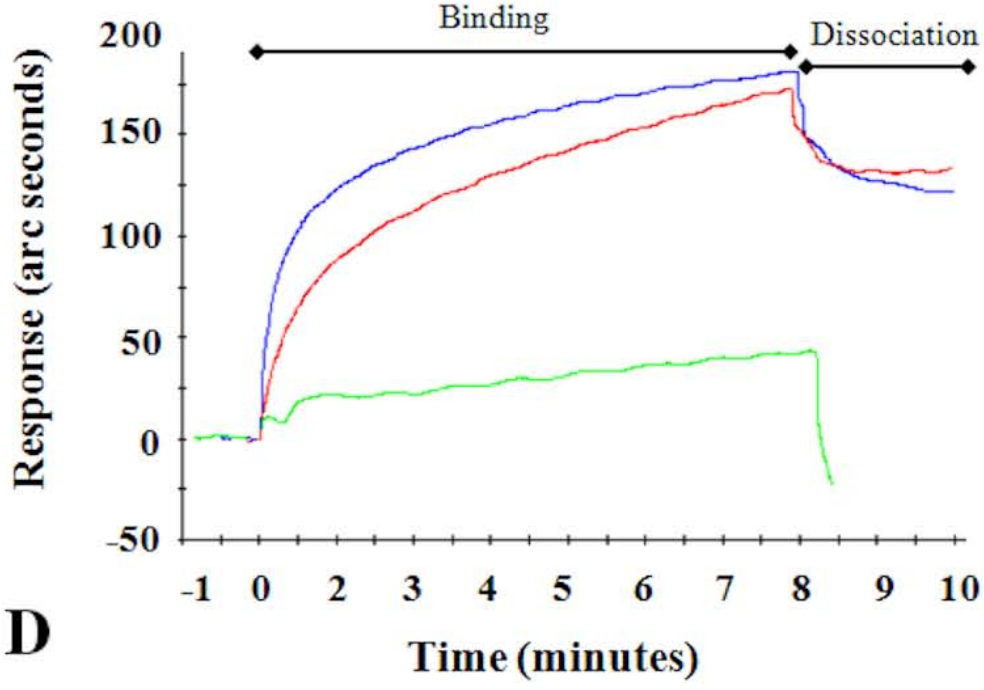

C

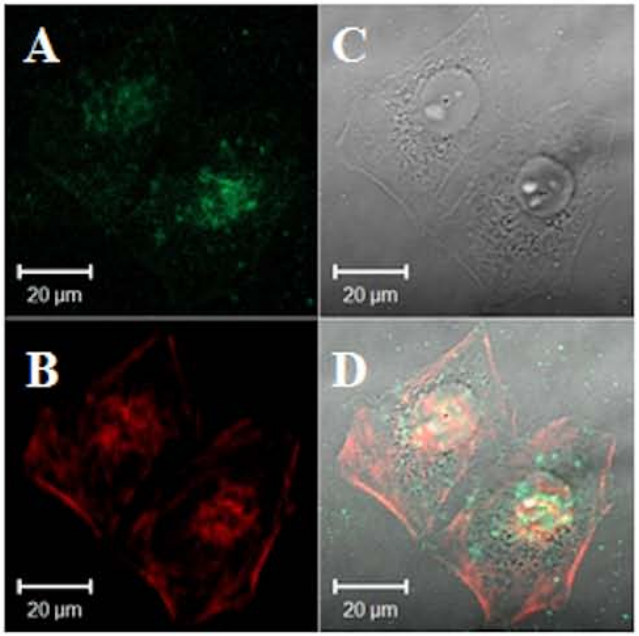

D

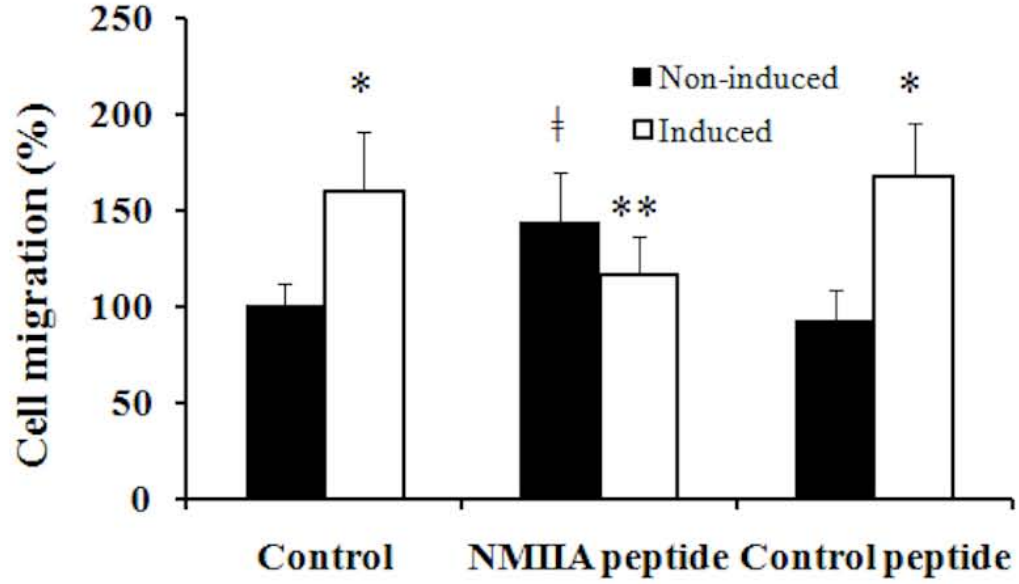

Figure 7

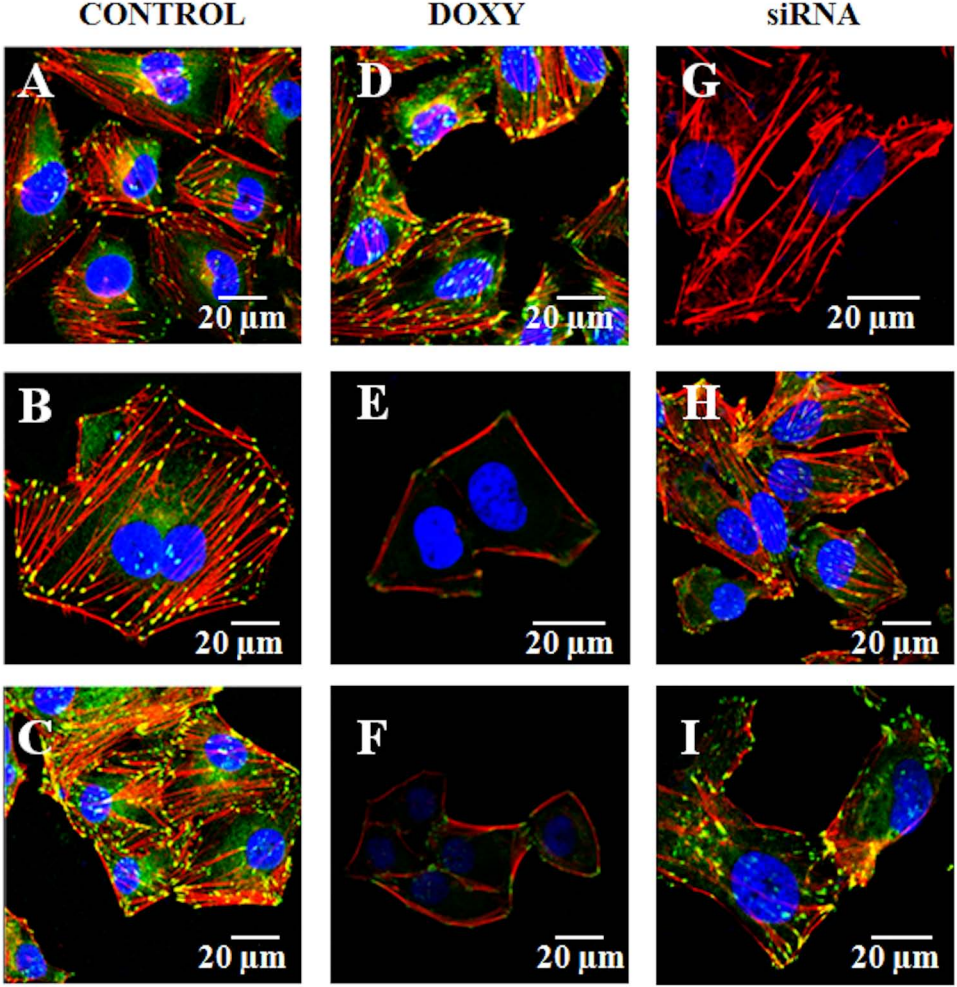
CONTROL
DOXY
siRNA
A
B
C
D
E
F
G
H
I
20 µm
20 µm
20 µm
20 µm
20 µm
20 µm
20 µm
20 µm
20 µm

Figure 8

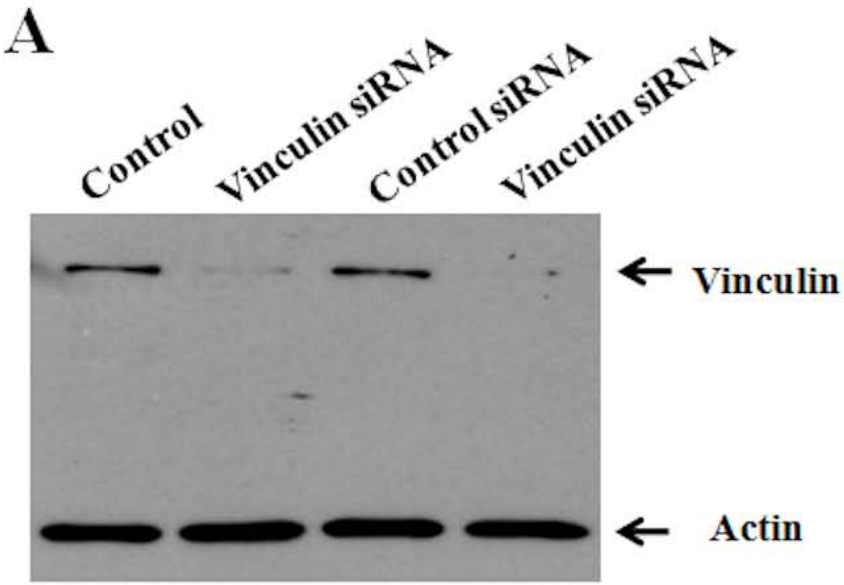
A
Control
Vinculin siRNA
Control siRNA
Vinculin siRNA
Vinculin
Actin

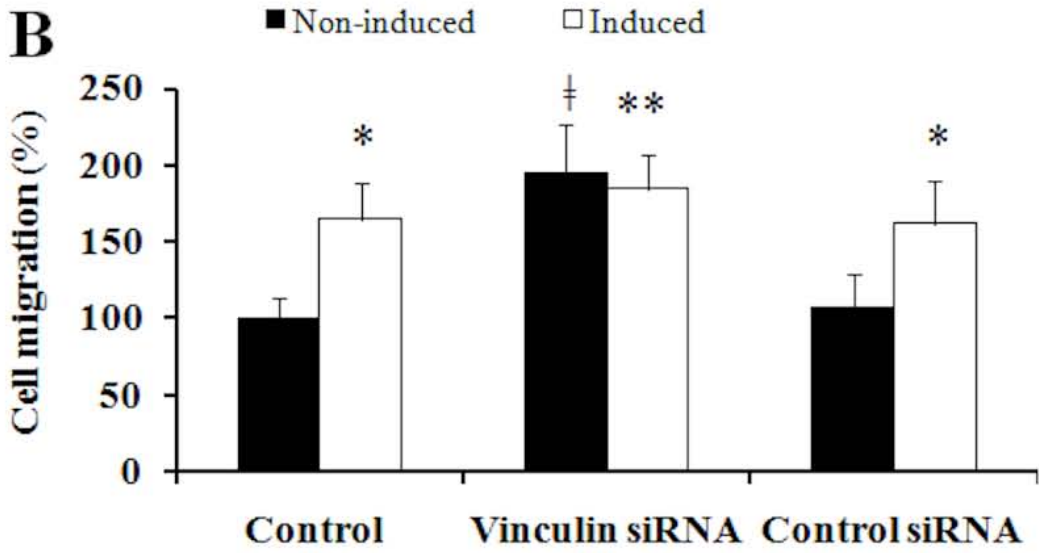
B
Non-induced
Induced
Cell migration (%)
250
200
150
100
50
0
*
‡
**
*
Control
Vinculin siRNA
Control siRNA

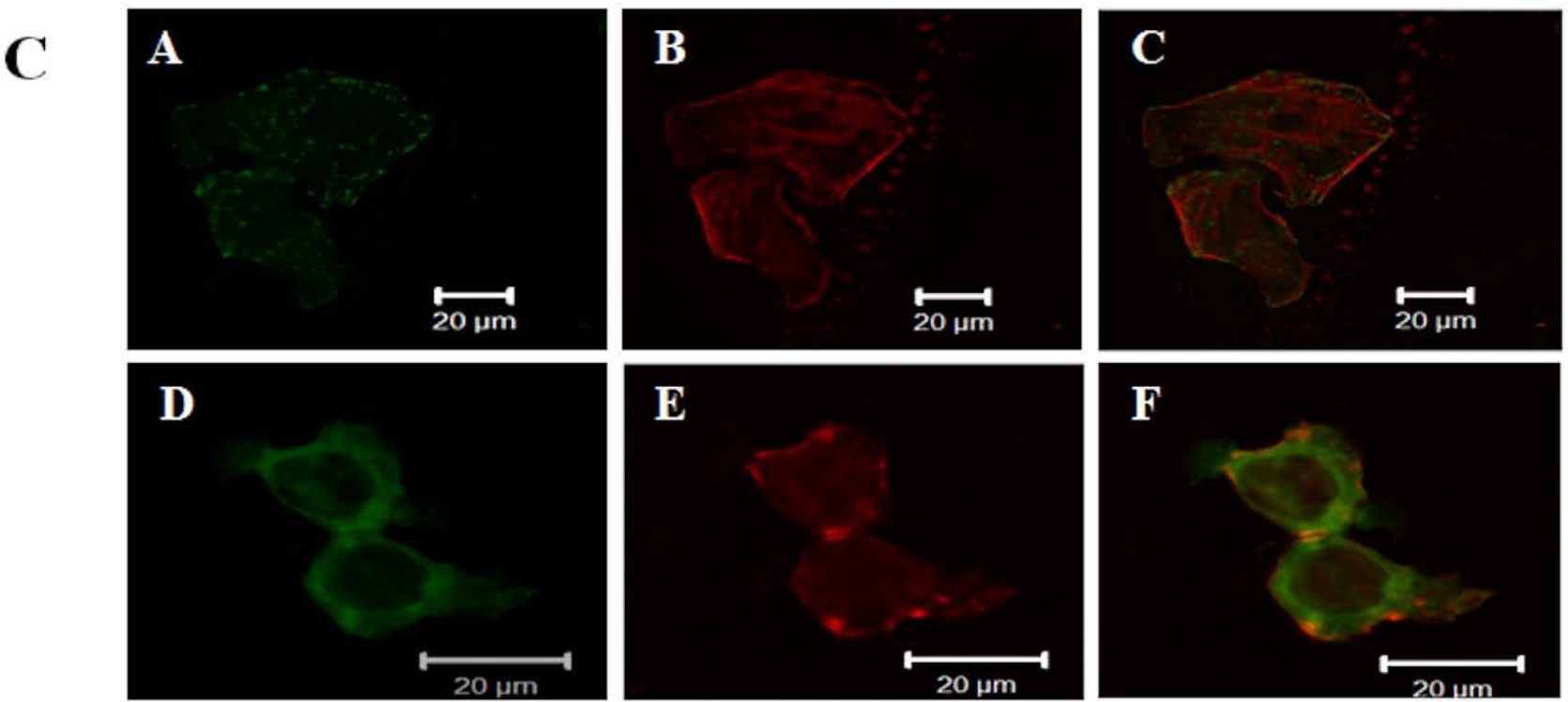
C
A
B
C
D
E
F
20 μm
20 μm
20 μm
20 μm
20 μm
20 μm

Figure 9

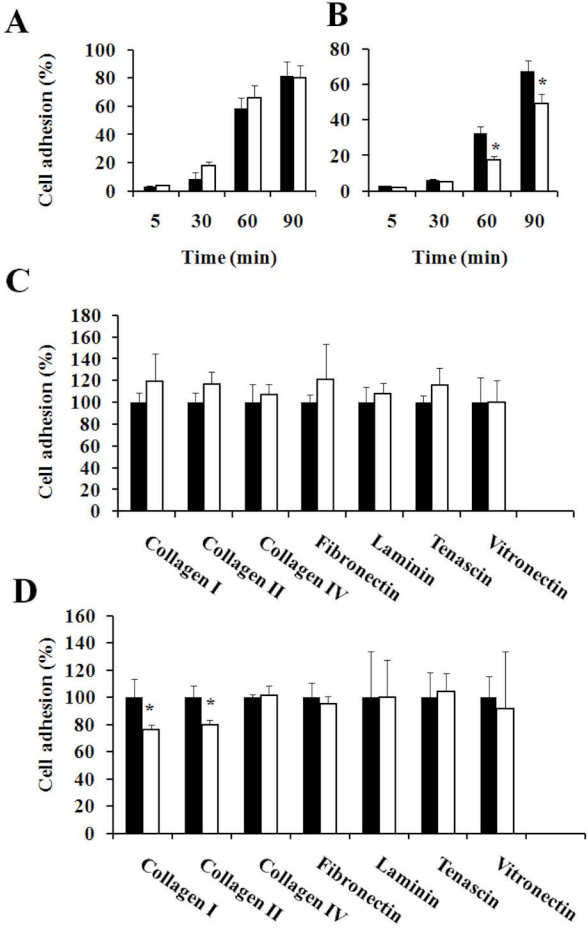
A
B
Cell adhesion (%)
100
80
60
40
20
0
5
30
60
90
Time (min)
*
C
D
180
160
140
120
Collagen I
Collagen II
Collagen IV
Fibronectin
Laminin
Tenascin
Vitronectin

Figure 10

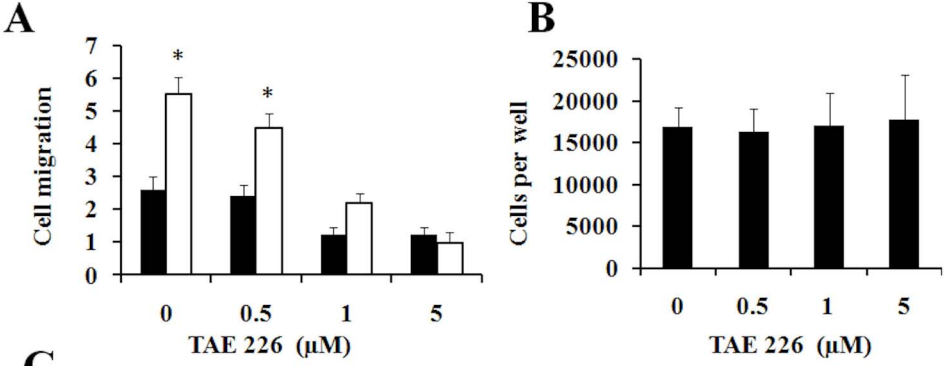
A
Cell migration
7
6
5
4
3
2
1
0
*
*
0
0.5
1
5
TAE 226 (μM)
B
Cells per well
25000
20000
15000
10000
5000
0
0
0.5
1
5
TAE 226 (μM)

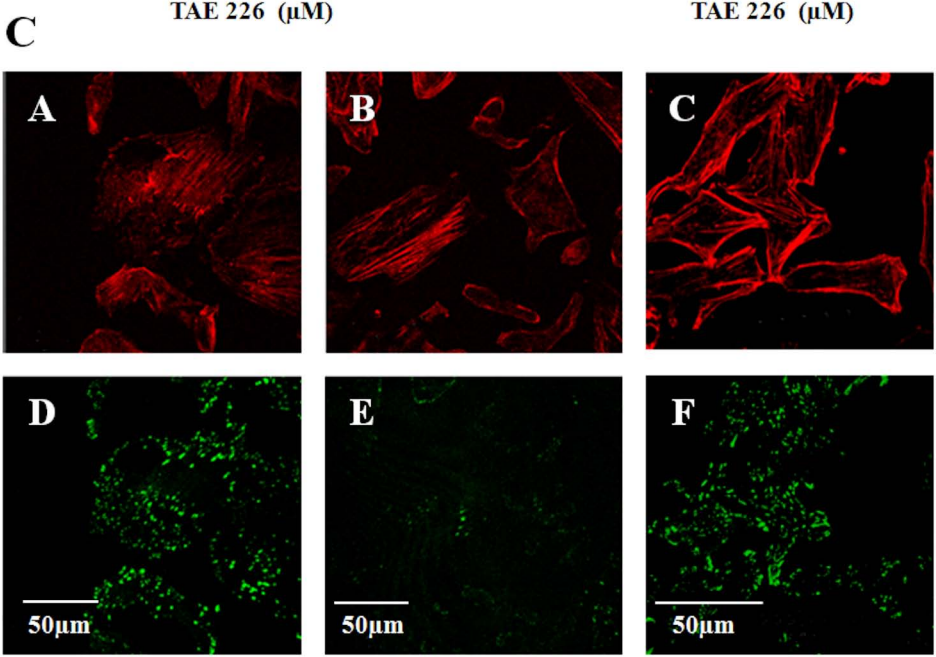
C
A
B
C
D
E
F
50μm
50μm
50μm